Energy Directors for Continuous Ultrasonic Welding of Thermoplastic Composites

MSc Thesis

Sanjeev Mohan

s.mohan@student.tudelft.nl
Aerospace Structures and Materials

TU Delft

Energy Directors for Continuous Ultrasonic Welding of Thermoplastic Composites

MSc Thesis

by

Sanjeev Mohan

to obtain the degree of Master of Science
at the Delft University of Technology,
to be defended publicly on 31st January 2019 at 10:00 AM.

Student number:	4627431	
Project duration:	November 2017 - January 2019	
Thesis committee:	Dr. ir. R. M. Groves,	TU Delft, Chair
	Dr. ir. I. F. Villegas,	TU Delft, Supervisor
	Dr. ir. J. M. J. F. van Campen,	TU Delft, External Committee Member

TU Delft

Abstract

Ultrasonic Welding (USW) is a rapidly upcoming technology for joining high performance Thermoplastic Composite (TPC) structures in the automotive industry. With the focus shifting from metals to composites for primary structures, USW process is seen as a fast, clean and efficient alternative for the conventional joining methods. Continuous Ultrasonic Welding (CUW) is an innovative, upscaled version of the USW process, where the weld is made over a moving part to create a weld line instead of a single spot.

Currently, there has been very limited research done in this field and the technology is in very early stages. The key to success of this technology lies in creating a uniform weld of an acceptable lap shear strength (LSS). Recent research has suggested that using a woven mesh as an energy director (ED) at the interface provides a good uniformity along the weld line, along with an acceptable LSS value. The research shows how the mesh deforms prior to the melting process, creating an intimate contact between the adherends and how this has a positive effect on the weld uniformity.

This study uses this data to design and manufacture a new ED that has these beneficial features incorporated in it. The study also uses an expanded mesh as an ED to study the effect of open areas in the weld uniformity. The EDs are used in the CUW process and compared based on their different features. Through this study, a deeper understanding of the behaviour of EDs during a CUW process is established which will be useful for developing new means of optimizing this process.

Acknowledgements

This report is a result of a year's work towards my graduation that started off as a literature study in the field. This work would not have been possible without the guidance and patience of my supervisor Dr. Irene Villegas, who always calmly guided me through the messy times and also provided with critical feedback on my work. I learnt a lot because of you, and I am very grateful for that.
Next, I would like to thank Dr. Roger Groves for taking time from his schedule to chair my graduation, and Dr. Julien van Campen for agreeing to be my external committee member.
Also, a big thanks to Tiago Felipe for attending my weekly meetings and providing a lot of useful tips throughout the course of this research.
My family has been my source of love and happiness, and none of this would have been possible if it wasn't for the amount of confidence they hold in me. It is their belief in me that keeps me going, even from a thousand miles away.
And lastly, my friends here have been like a family away from home. You made my life here beautiful, thanks!

Sanjeev Mohan

Contents

List of Figures

List of Tables

1

Introduction

Air traffic is on a constant rise, with air travel being the preferred means of travel for both short and long distances. To make air travel economical and environment-friendly, it is vital for the aircrafts to operate efficiently. One way of improving the efficiency of aircrafts is by making them lighter, which would, in turn reduce their fuel consumption.

Fibre reinforced composites (FRC) offer a solution to this problem because of their high specific strength and stiffness compared to the existing options. FRCs are being increasingly used in the automotive and aerospace industries for structural applications because of this reason, and there is extensive research being done to implement them in a variety of applications. One of the factors that majorly affects their implementation in the industry is their manufacturability: realizing FRCs into actual structures can be tedious because of their heterogeneity when compared to their metal counterparts. It is hence necessary to investigate the optimization of the manufacturing processes to achieve perfect composite structures with the least possible effort.

Carbon fibres (CF), Glass fibres (GF) and Aramid fibres are commonly used to reinforce a polymer resin base. The polymeric resins are classified into thermoplastics (TP) and thermosets (TS), which based on the ability of the polymer chains to form physical bonds among themselves. The physical bonds in thermoplastics are breakable, meaning they can be reconsolidated into different shapes by applying the right amount of energy while maintaining their initial mechanical properties. This opens up options for manufacturing processes like fusion bonding, and welding which is not possible in heavily cross-linked polymeric chains of thermosets. Combined with their comparatively superior mechanical properties and ease of storage, thermoplastic composites (TPCs) offer many prospective solutions for upcoming structural requirements of the industry.

Fusion bonding techniques involves heating the polymeric resin at the interface to a molten state, and then allowing for the chains to diffuse from one side to the other resulting in a seamless joint. This process can be classified on the basis of the mechanism used to generate the heat at the interface: thermal, friction or electromagnetic[29].

Ultrasonic welding (USW) is a fusion bonding technique that has been used in the industry to join plastics since the 1980s after it was patented by Robert Soloff and Seymour Linsley[16] in 1965. The process uses the friction at the interface due to vibrations at ultrasonic frequency to generate heat and form a fusion bond. The process is quick, neat and has a lot of scope for automation[15], [21] and the resulting welds are seen to have a strengths and qualities analogous to compression moulded structures[9].

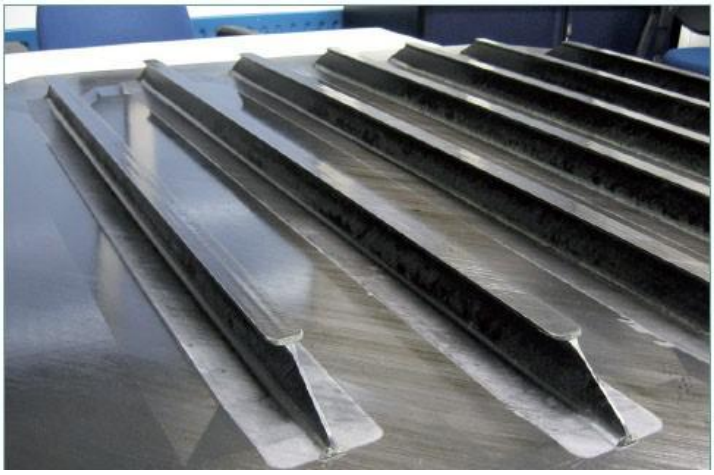

Figure 1.1: A possible application of an upscaled USW process is the skin-flange interface of a skin stiffened structure

By nature, USW is a spot welding process and is analogous to a mechanically fastened joint. USW spot welded joints in TPCs are found to be very effective, with their strengths comparable to riveted joints when loaded in-plane[30]. The spot welding process can be upscaled to cover larger areas,as shown in Fig.1.1 in two ways: a sequential way and a continuous way. As the name suggests, sequential USW involves multiple spot welds one next to the other to form a continuous weld line.
Continuous Ultrasonic Welding (CUW) for TPCs on the other hand is relatively new and there is a lot of research yet to be done before it can be applied in the industry. This process is carried out by moving a sonotrode on the overlap at a constant speed to generate heat along the weldline and hence promote a fusion bond. Continuous welds are needed at locations where having stress concentrations and local buckling are undesirable, such as the case of a skin-stiffened structure.
At the current state of art, CUW is not ready to be applied at an industrial level because of the lack of research. The process is complex to understand, with some of the data being generated from the process being difficult to comprehend. This opens up a lot of opportunities for research by trial and error, by understanding what the ”good” parameters for the process are and how they affect the process. There has been very limited research on improving the quality of the continuous weld by altering the features of the interface. This study tries to build on these available data by extrapolating their results and applying them in a different way.
In this study, the quality of a continuous weld is monitored by altering the structure of an energy director at the interface of the joint and the results are used to find a correlation between them.

2

Literature Study

The first step towards the research was to get acquainted with field and familiarized with the research that has been done so far in the field. A literature study was hence performed, and is summarized in this chapter.

2.1. Ultrasonic Welding

Ultrasonic welding is a fusion bonding process that uses friction to generate the heat required to carry out the fusion process between the two substrates. The friction is induced by a sonotrode vibrating at an ultrasonic frequency while applying a certain amount of force on the overlap. A schematic diagram of the working of an USW machine is shown in Fig.2.1, and the setup of the substrates is shown in Fig.2.2

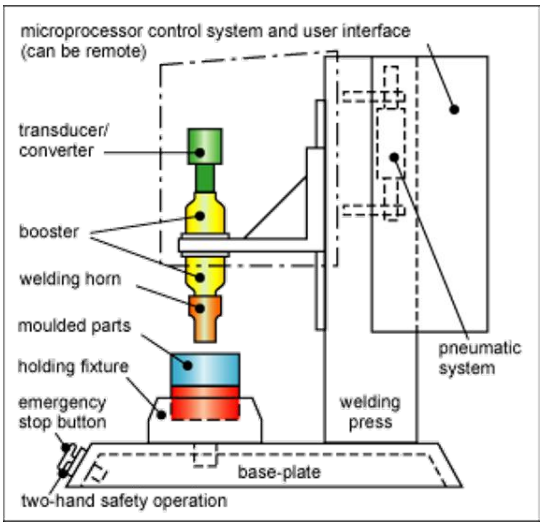

Figure 2.1: The principle behind the working of a ultrasonic welding machine[22]

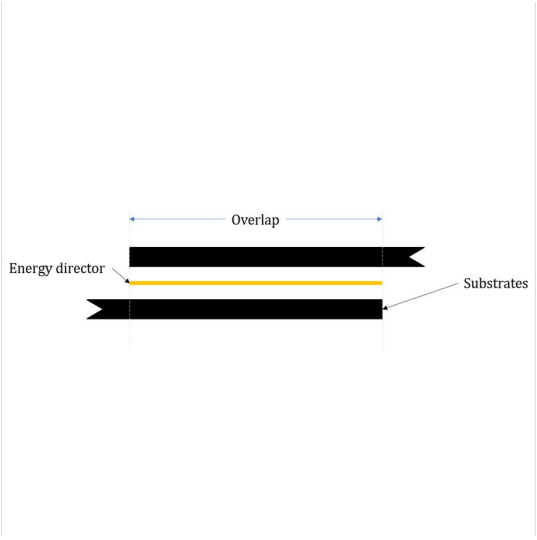

Figure 2.2: A layer of neat resin is used between the substrates to initiate the melting process

The amount of force exerted by the sonotrode has an effect on the energy transmission of through the material[15], which in turn affects the weld quality of a plastic joint. When it comes to a composite joint, there is limited literature available and some trials required to determine the ideal welding force. Hence, for this research, forces that have already been tried in previous research were used to keep the focus on ED behaviour.
As for the welding process itself, it can be divided into two phases: the vibration phase and the solidification phase. The vibration phase is characterized by the motion of the surfaces already under the joining pressure, in order to generate heat by friction. The weld frequency

is usually in the range of 20kHz to 50kHz and the amplitudes vary between 2.5µm to 250µm [3]. The resulting molten resin at the interface then wets the joint surface and facilitates the intermolecular diffusion to form a joint between both the substrate surfaces. The following solidification phase primarily consists of the resting of the moving polymer chains in the molten resin at the interface at the constant joining pressure, resulting in a welded joint. The whole process can be broken down into five different subprocesses:

1. **Mechanics and vibration**
   This subprocess relates to the joining pressure and the vibrations exerted by the sonotrode over the surfaces. The strain distribution among the energy directors can be usually predicted by creating an equivalent mechanical model using a lumped parameter system which considers all the inertial effects of the moving parts as well as the effects of the static joining pressure.

2. **Viscoelastic heating**
   Viscoelasticity is the property of a material which allows it to exhibit both viscous and elastic properties when undergoing deformation. The vibrations from the sonotrode cause cyclic strains in the energy directors, which then gets converted into heat because of the intermolecular friction. The viscoelastic heating rate is given by the following equation[3]:

$$\dot{Q_v} = \frac{\omega.\epsilon_0^2.E''}{2} \tag{2.1}$$

   where $\dot{Q_v}$ is the viscoelastic heating rate; ω is the frequency of vibration; ϵ_0 is the cyclic strain of the energy directors and E" is the loss modulus of the polymeric resin. Given its dependence on the loss modulus, the viscoelastic heating is only significant once the temperatures have reached the glass transition (T_g) of the polymeric resin. This temperature is reached with the help of interfacial friction between the surfaces, which generates the necessary heat[3].

3. **Heat transfer**
   This process relates to the transfer of the heat generated by the energy directors to the substrate surfaces. The thermal conductivity of the composite also plays an important role in the heat transfer, since most of the heat is transferred through conduction. This means that a carbon fibre composite will exhibit better heat transfer compared to a glass fiber composite, which would in turn lead to quicker heating of the resin and hence shorten the total weld time.

4. **Flow of molten polymer**
   Once the polymeric resin at the interface is molten, it needs to wet the entire surface to form a good quality weld. The wetting of the joint strongly depends on the squeeze force since the viscosity of the melt is very high. The flow can be modelled by treating it as a spring system where the molten resin is first analogous to a spring that starts getting stiffer as the flow progresses and covers the entire surface. After this point, the entire substrate system starts vibrating along with the sonotrode.

5. **Intermolecular diffusion**
   A continuous joint is created when molecular chains from both the substrates and the energy directors diffuse into their counterparts. For amorphous polymers, the diffusion time depends on the respective polymer's glass transition temperature. The higher the temperature, the quicker the diffusion takes place. The diffusion time of semi-crystalline polymers is noted to be of the order of 10^{-7} seconds[11], which is around a 6^{th} of the order of magnitude of the welding times, meaning that diffusion is not limited by the welding time.

2.1.1. Process monitoring

Process monitoring for ultrasonic welding in composites is slightly challenging since there is no foreign material allowed at the interface. This eliminates the use of devices such as thermocouples, where in the probes get left behind at the interface. A study performed by Irene Villegas and Genevieve Palardy found a relation between the transformations at the inteface and the dissipated power (and the displacement of the sonotrode)[25]. This relationship can be used to define the optimal processing parameters for a particular welding setup.
The power and displacement variation of the sonotrode can be plotted against time, and the resulting curve is often referred to as the 'power-displacement curve'. A typical example of such a curve is shown in Fig. 2.3.

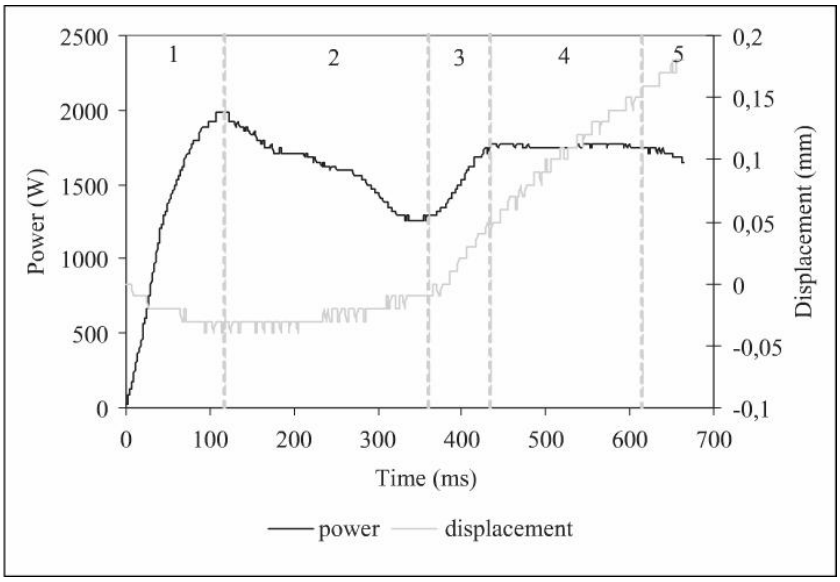

Figure 2.3: A typical example of the power displacement curve obtained for a lap joint of CF/PEI composite panels. Positive displacement values indicate downward movement of the sonotrode[25]

The curve can be demarcated into 5 different stages as shown in the figure, based on the process taking place at the interface:

1. In the first stage, the power is increased in a ramped manner, and the sonotrode retracts slightly to accommodate the vibration. There is no noticeable change to the shape of the energy directors in this phase.
2. During the second stage, a decrease in the power is noticed, which is attributed to the fact that the solid contact area reduces due to melting in isolated spots over the energy directors. The displacement of the sonotrode however does not vary much because of the presence of unmolten areas along the weld lines.
3. The third stage begins with all the energy directors molten, and is characterized by the squeeze flow of the melt between the substrates. This results in an increase in the sonotrode displacement and an increase in the power dissipated because once the molten flow fronts meet, the mechanical impedance of the joint increases.
4. During the fourth stage, the squeeze flow of the resin continues with the weld line thickness approaching zero. The heat transfer from the molten resin also causes some of the resin from the substrates to melt.
5. The fifth and the final stage is characterized by the melting of the resin beyond the first few layers of the substrates which causes a slight dip in the power dissipation as observed in the second stage. Distortion of the shape of the fibre bundles is also observed in this stage.

2.2. Energy directors

So far, it has been established that energy directors are needed to initiate the melting process at the beginning of the weld. This subsection is elaborates a bit more about this based on the available literature.

Energy directors are resin rich asperities placed on the welding interface, to induce the melting process at the interface. Because of their lower stiffness, they have a higher cyclic strain and hence melt much faster than the rest of the overlap. The partially molten resin has an even lower stiffness and further creates heat to melt the interface through visco-elastic friction. The resulting weld is seen to have a better quality.[2]

Energy directors can be manufactured in different shapes, and there has been studies relating the shape and the weld quality achieved as a result of having that shape. An example of the effect of geometry of an energy director's contact point is shown in Fig.2.4.

Figure 2.4: The effect of having a sharp and a rounded energy director on the weld quality of the joint. (Copyright: Dukane Corporation [6])

The shape of the energy director has an effect on how quickly the melting process is initiated. For example, a study found that a rounded ED requires a larger vibrating amplitude than a sharp ED to achieve the highest joint strength[18]. This implies that a design that has a higher contact pressure will need a lower welding amplitude. Another study[4] carried out on the shape of the energy directors identifies the most efficient geometry. A comparison is carried out between three geometries: triangular, rectangular and semi-circular.

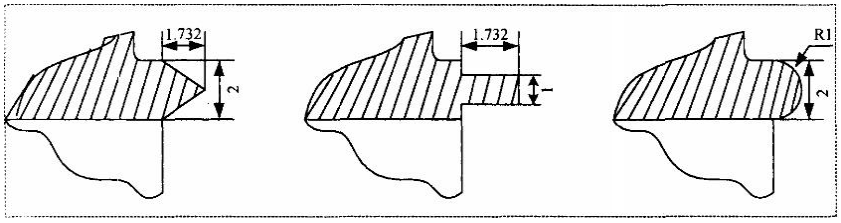

Figure 2.5: The energy director shapes as compared by Chuah et al. [4]

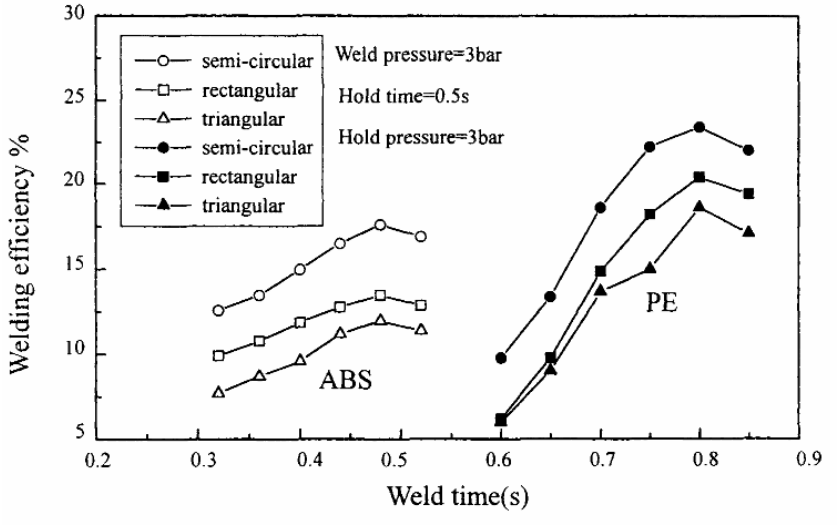

Figure 2.6: Welding eficiency versus weld time(ABS: Acrylonitrile buta- diene styrene, amourphous and PE: Polyester, amorphous [4]

Looking at the graph shown in Fig.2.6, when compared on the basis of welding efficiency (defined as the strength of the weld divided by the strength of the parent material), the semi-circular contact surface was found to be the best, followed by the rectangular one and the least efficiency was attained by having triangular energy directors.
However, it has to be taken into consideration that these results are only valid for plates thicker than 6mm. This means that the plates are quite stiff and rigid during the welding process, and do not deform much. Hence, the validity of these results to thinner plates is questionable, and needs to be evaluated.
A study using Finite Element Modeling for the energy directors found that for triangular energy directors, the apex angle has a significant effect on the heating at the interface. It was found that with an increase in the apex angle, the glass transition temperature was reached quicker, with the most efficient angle being at 90°. [28].

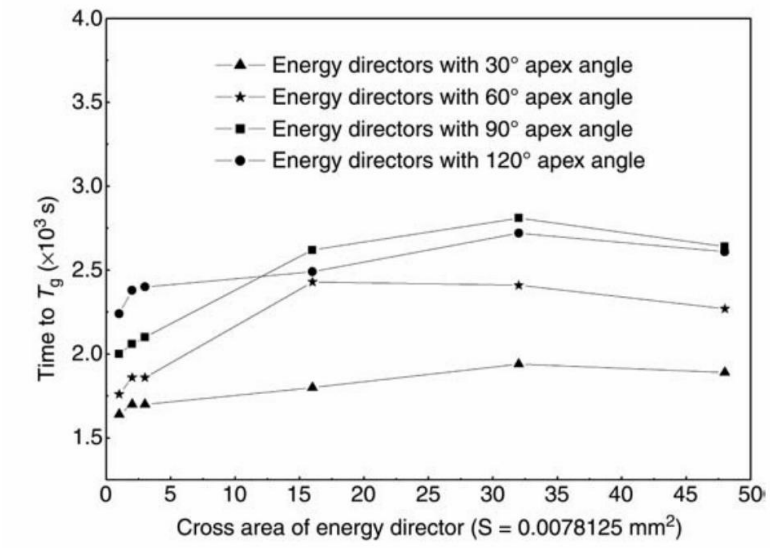

Figure 2.7: Time to reach the T_g of the energy directors with different energy director cross-section areas and apex angles. (S being the initial areal width of the contact area, set to constant for this study) [28]

Another interesting aspect of this study was the dependence on the cross-sectional area of the energy director. A larger cross-section implies a longer welding time, whereas a smaller

cross-section can cause too much heat to be dissipated into the laminates. Hence an optimum cross-section area has to be calculated, which in this case was found to be $0.25mm^2$ for an apex angle of 90^o.[28]

2.3. Manufacturing options for energy directors

This part of the literature study was aimed at gathering information on different ways to manufacture an energy directing surface for USWs. Two approaches were explored and implemented:

- Fused Deposition Modeling
- Moulding

2.3.1. Fused Deposition Modeling

Since the energy directors are also made of thermoplastic polymers, FDM can be implemented to apply them on to composite surfaces.

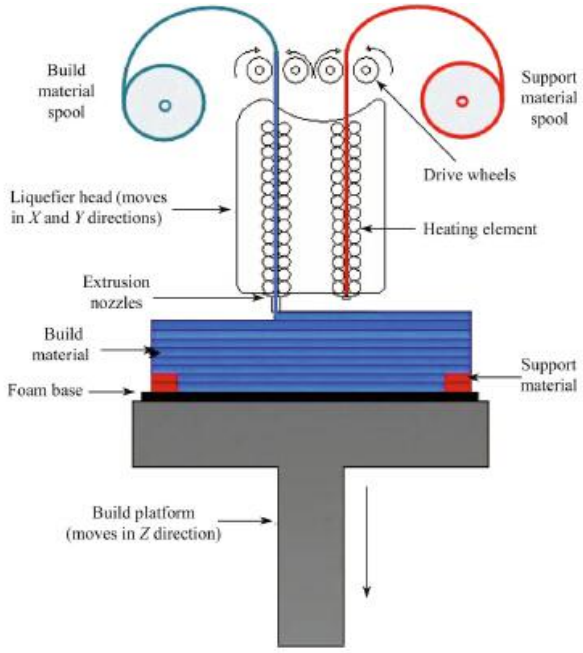

Figure 2.8: A schematic depicting the working principle of an FDM process.[13]

The use of FDM for making energy directors has been explored by M.A.P. Kerssemakers et al. It was noted that when using a PEEK ED on a CF/PPS substrate, there was no further steps required to fixate the ED, however this was not the case with a CF/PEEK substrate which showed insufficient adhesion[12]. Another challenge faced during this process was the inconsistency in the thickness of the extruded EDs, which could have significant effects on the final weld quality.

2.3.2. Moulding

The required energy directors could be manufactured on the surface using a custom-made mould that can heat up to temperatures above the T_g of the polymeric resin to allow reshaping but lower than the T_m to prevent excess flow. A similar process was used to manufacture triangular energy directors in a study by Avraham Benatar [3] and Irene Villegas [26], and was found to be effective. A metallic mould can be manufactured using a machining operations or a CNC mill depending on the level of complexity of the design. Fig.2.9 shows an example of moulded triangular energy directors created on the surface using two thick aluminium plates with triangular grooves machined onto them[27].

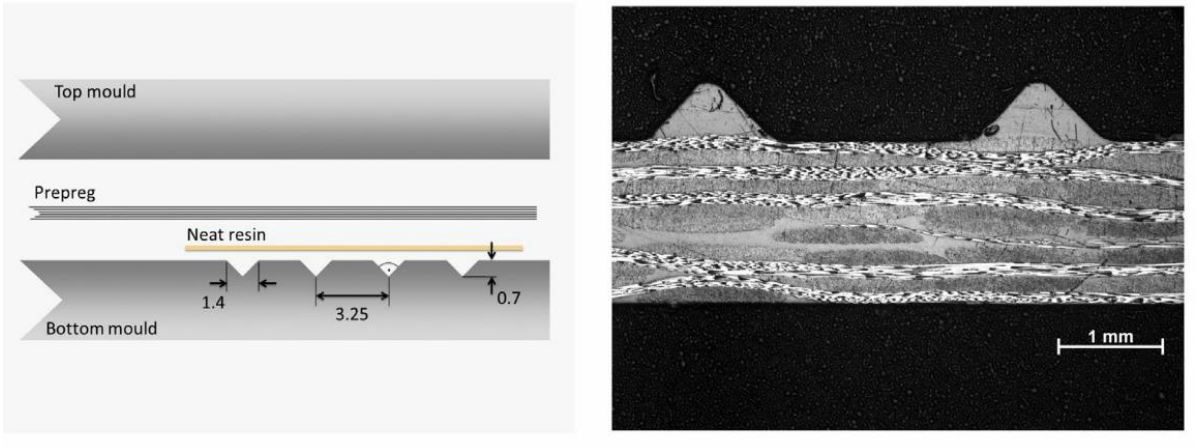

Figure 2.9: Moulded triangular energy directors[27]

2.4. Continuous Ultrasonic Welding

Continuous Ultrasonic Welding (CUW) is a relatively new technology for thermoplastic composites, which still needs a lot of research before it can be effectively applied in the aerospace industry. The techniques used for this process have largely been developed in-house at DASML. The first welding fixture in DASML for CUW was developed in 2015, and was capable of moving the sonotrode horizontally over a fixed table[23]. Using this fixture, research was conducted to check the feasibility of the CUW process by minimising the squeeze force of the molten resin to zero[19]. The squeeze force was minimized by making the net displacement (travel) of the sonotrode to zero, meaning the sonotrode vibrates at the same vertical position throughout the welding process. A zero-travel USW takes into account the unmolten ED lying ahead of the molten ED, which is usually thicker, as shown in Fig.2.10.

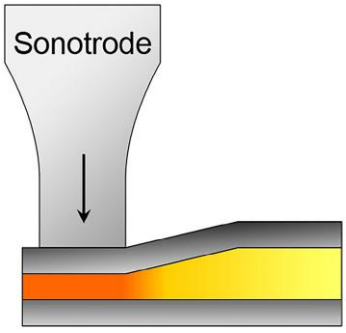

Figure 2.10: Unmolten resin in front of the weld during a CUW process[20]

The research uses laminates made of Carbon-fiber/Polyphenylene sulfide (CF/PPS) and a flat ED made of PPS to make the weld. Although the resulting fracture surfaces showed areas of intact resin, the zero-travel concept showed that a CUW process in fact feasible for thermoplastic composites. A later research went on to show that using a mesh-type ED resulted in CUWs of with better weld uniformity compared to a flat ED of the same resin volume[10]. It was concluded that the filament crossings in the mesh resulted in a better contact between the substrates which in turn resulted in a more uniform heat generation. Fig.2.11 shows how the meshes deform before melting to create an intimate contact between the substrates.

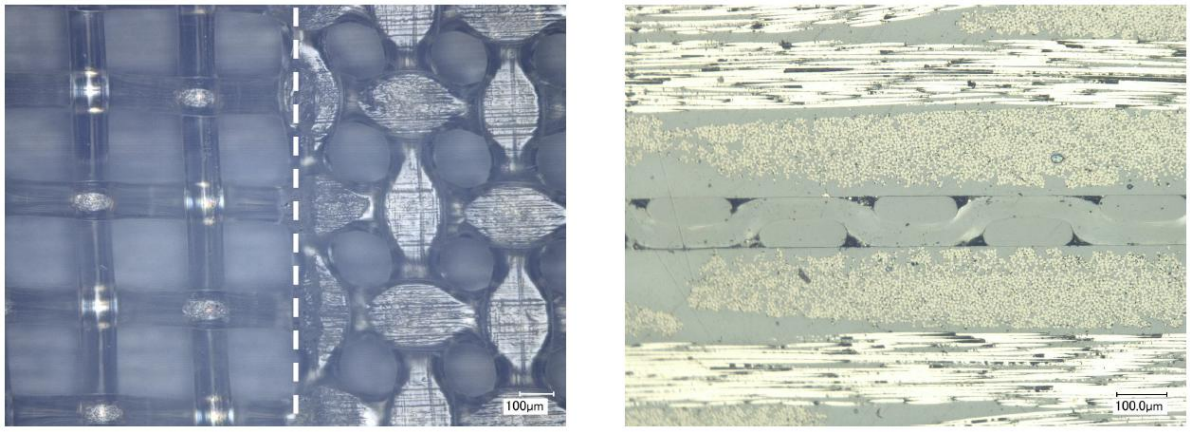

Figure 2.11: The mesh deforms under the welding force to create a uniform contact between the substrates[10]

2.5. Conclusions from the literature survey

The aim of the literature study was to get familiar with the field of ultrasonic welding of thermoplastic composites. Firstly, a deeper understanding of the process was gained by studying the different stages of the power-displacement curves and correlating them with the changes happening at the interface. Then, the role of energy directors was studied and the effect of the shape on the welding process was understood. The next step was to explore the different ways in which the EDs could be manufactured at the DASML. Two options were set up: a fused deposition model and a moulded option. The final part was to go through the previous researches to determine which features are beneficial for a CUW. It was concluded that to get a good weld-line uniformity, the ED should have features similar to that of a woven mesh, which are:

- Small contact points
- Homogeneous spread of these contact points
- Some displacement prior to melting, to create an intimate contact between the substrates(preforming)

The design of the EDs in the upcoming chapters is made keeping these factors in mind.

2.6. Research goals and objectives

The primary aim of this research is to design and manufacture an energy director interface that can produce better quality continuous ultrasonic welds by aiding uniform heat generation and a high lap shear strength. The main research question that needs to be answered through this study is:

"What are the physical features of an energy director that affect continuous ultrasonic welding of thermoplastic composites? And what is their effect?"

The answer to this question will be attained by using the existing data on continuous ultrasonic welding of thermoplastic composites to identify the features that have an effect on the process, and then manufacture an energy director that incorporates these features. These energy directors need to be welded at different speeds to understand their behaviour. Hence, the research objective can be formulated as:

"The objective of this research is to understand the behaviour of an energy director during continuous ultrasonic welding process and manufacture a design that results in a weld with uniform heat generation throughout the weld."

This objective can be broken down into the following subquestions:

- What are the desirable features of an energy director that result in a good continuous ultrasonic weld?
- How can these features be incorporated into a new design?
- How can this design be manufactured?
- What is the relation between the physical features of an energy director and the final weld quality?

These questions are answered as per the methodology explained in the next section.

2.7. Methodology

This section explains the path followed during the course of the research to answer the research question. Fig.2.12 shows a general overview of the steps taken to do this.

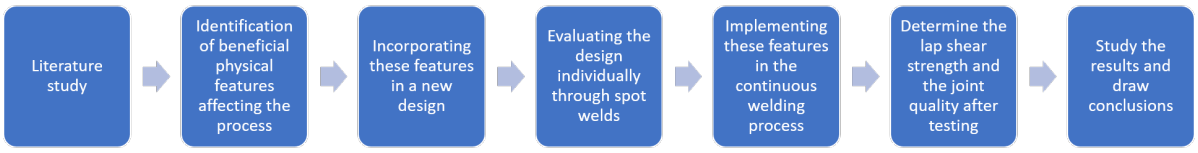

Figure 2.12: The research methodology followed throughout this study

The first step is to conduct a literature survey to identify the physical features of an ED that seemingly have a positive effect on the weld quality, and to gain a deep understanding of the process itself. The literature also provides some good information about the processing parameters that could be used for this research.
Once there is a good idea about the beneficial features for an ED for CUW, the next step is into a design that is manufacturable at the DASML. This design is then manufactured after some trials to get a proof of concept for the manufacturing method. After this, an accurate version of the design is manufactured and used for spot welds. The spot welds give information about the power-displacement behaviour of the spot welds and provide reference for the lap shear strengths.

The next step is to use this ED in a CUW process after figuring out a range of welding speeds that would work on PEEK EDs. This is done by carrying out smaller welds of 101.6mm length over a wide range of speeds. Once there is an idea about the welding speeds, longer welds of 220mm are made to have a clear picture of the EDs behaviour under CUW.
To see the results, the weld needs to be tested for its LSS and for its fracture surface. The fracture surface gives vital information about the heat generation at the interface and the resin cover in the overlap. The LSS is an indication of the strength of the joint for each ED type and welding speed. With this information, conclusions are drawn from the results and some recommendations are given for the future research.

3

Experimental Setup

The aim of this chapter is to provide a summary of the materials, techniques and equipment available at the Delft Aerospace Structures and Materials Laboratory(DASML) used for carrying out this research.

3.1. Materials

3.1.1. Substrates for spot welds and CUW

The substrates for welding were cut from two different types of laminates: a [0/90]3s 5-harness satin weave carbon fibres embedded in a polyether ether ketone matrix (CF/PEEK) and a $[0/90]_{3s}$ 5-harness satin weave carbon fibres embedded in a polyphenylene sulfide matrix (CF/PPS) supplied by TenCate Advanced Composites. For both the laminates a hot-platen press was used for consolidation as per the press cycles shown in Table 3.1.The thickness of both the CF/PEEK and the CF/PPS laminates was around 1.9mm.

	CF/PEEK	CF/PPS
Temperature [°C]	385	320
Consolidation Time [min]	20	20
Pressure [MPa]	2	1

Table 3.1: The consolidation scheme used to prepare the laminates

The laminates were then cut into the final dimensions using a water-cooled a surface grinding machine manufactured by Proth Industrial Co. Ltd., with a 100µm depth of cut. For spot welds, the laminates were cut into samples of 101.6 x 25.4mm. For the CUW, samples were cut into dimensions of 101.6 x 101.6mm for estimating the welding speed, and 101.6 x 220mm for longer welds that were used for comparison.

3.1.2. Energy directors

PEEK and PPS EDs were used for this research. The use of PPS EDs was limited to the initial validation of the conical design, that is, to make a proof of concept for the mould and to check for a relation between the cone height and the preforming. For the woven mesh option, a PEEK mesh provided by PVF Mesh & Screen Technology GmbH was used as an energy director at the interface. The mesh has a thickness of 0.2mm and a mesh count(warp/weft)[17] of 155/37 per square cm. The mesh has a 37% open area.
An expanded PEEK mesh of 0.14mm thickness provided by Dexmet Corporation was later used as an ED. The expanded mesh is manufactured by simultaneously slitting and stretching a thin film[5] of PEEK resin, as shown in Fig.3.1. Compared to the woven mesh, this option has an open area of 62%.

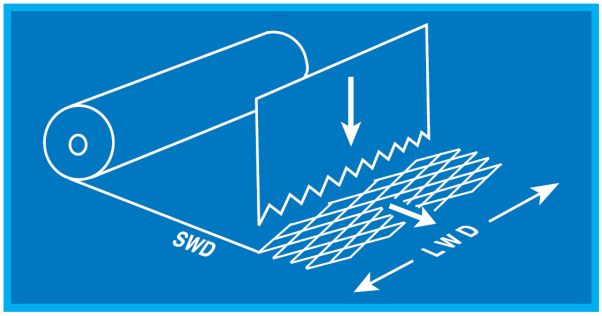

Figure 3.1: The manufacturing process of a PEEK expanded mesh[5]

A conical design was manufactured at the laboratory using an Aluminium mould with resin films of PEEK and PPS in a hot platen press. The mould was made using a bench drill on a 3mm thick Aluminium sheet. The PEEK films used for this purpose were 0.05mm thick and supplied by Victrex Plc, UK. The PPS films used here were 0.08mm thick and supplied by TenCate. More details about the manufacturing process are explained in the following chapters.
Fused Deposition Modelling (FDM) was used to create strips of PEEK on the beforementioned PEEK film of 0.05mm thickness. The FDM process was carried out using an Indmatec HPP155, designed by Apium Additive Technologies GmbH in Germany. The machine uses 1.75mm diameter filaments as raw material which is pushed out through a nozzle at 400°C. The bed can be heated up to a temperature of 100°C and offers an effective build volume of 140 x 135 x 148mm.

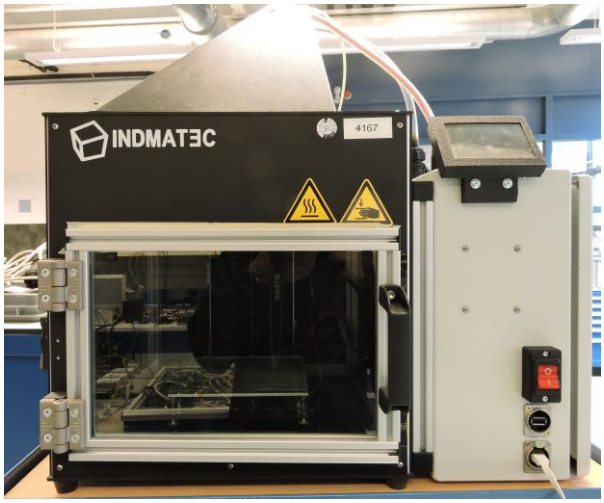

Figure 3.2: The PEEK 3-D printer used for the extrusion process

3.2. Ultrasonic Welding - Spot welds

For the spot welds made during the course of this research, Hermann Ultraschall HiQ Dialog machine welding machine was used, which has a maximum output of 6200W. An in-house built fixture was used to hold the specimens in place, which is shown in Fig.3.3. Throughout this research, a 30mm x 15mm rectangular sonotrode was used for making the spot welds, and the parameters shown in Table 3.2 were used.

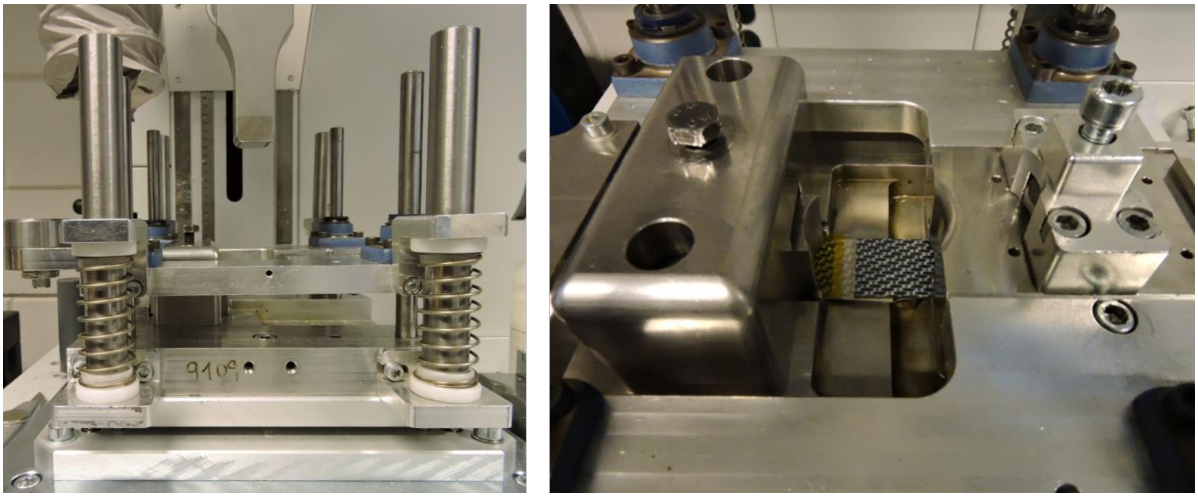

Figure 3.3: The welding fixture used for making the spot welds (left) and the loading of the specimen (right)

Parameter	Setting
Frequency [kHz]	20
Peak-to-peak Amplitude [µm]	86.6
Weld Force [N]	500
Solidification Force [N]	1000
Solidification Time [ms]	4000

Table 3.2: The welding parameters used to make the spot welds

The optimum welding parameters are determined using the in situ data from the ultrasonic welder. The spot weld is first done using a displacement controlled method, wherein the sonotrode is allowed to travel a distance equal to 80% of the thickness of the ED. Using the data from this welding, the different stages of the welding are identified. Prior research with a CF/PEI laminate and a flat PEI ED revealed that the optimum welds are obtained at the end of the 4^{th} stage of welding[24] which is characterized by a simultaneous flow of molten ED and melting of the first surfaces of the substrates. This occurs when the sonotrode has travelled roughly 20% of the thickness of the ED, and can be identified in the power curve when the second peak has been crossed.
Fig. 3.4 (left) shows an example power-displacement curve of a USW of CF/PEI using a flat PEI ED, along with the position of the second power peak[14]. Identification of an analogous spot in the graph of a weld with a mesh-type ED is slightly different, since the second power peak is not as prominent. A typical power-displacement graph is shown in Fig.3.4 on the right, by welding a CF/PPS laminates with a PPS mesh as an ED.

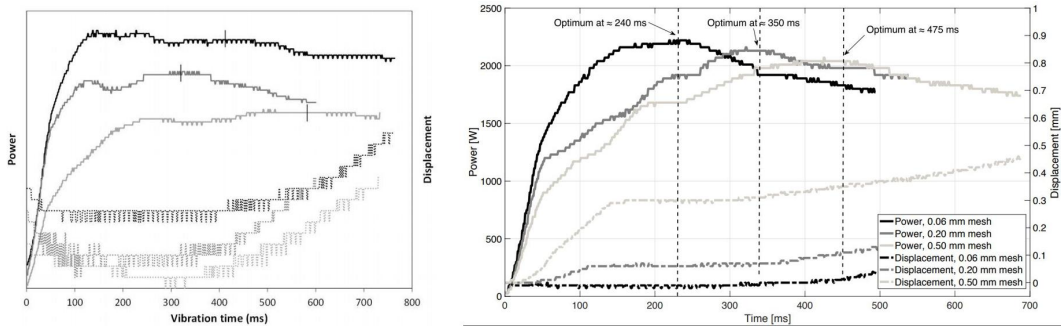

Figure 3.4: A typical power-displacement curve of a spot weld with a flat ED at the interface(CF/PEI with a 0.06mm thick flat PEI ED)[14](left) and A typical power-displacement curve of a spot weld with a mesh ED at the interface (curves for three different thicknesses are shown, CF/PPS substrate and PPS mesh)[10] (right)

Research suggests that the optimum weld for a mesh-type ED is at the point where the displacement starts to increase after the plateau, as marked in the figure.Once the optimum points have been found in the curve, the time is noted down and used to carry out time-controlled welds using the same other parameters. When welded for the optimum time, the resulting welds should ideally have the highest possible LSS for the case and hence can be used as a reference.

3.3. Continuous Ultrasonic Welding

For CUWs, an in-house built welding setup is used along with an in-house built fixture to hold the specimens. The setup is loaded with a Hermann Ultraschall Dialog 6200, which has a maximum output of 6200W. The welding setup and the fixture used for all of the continuous welds is shown in Fig.3.5

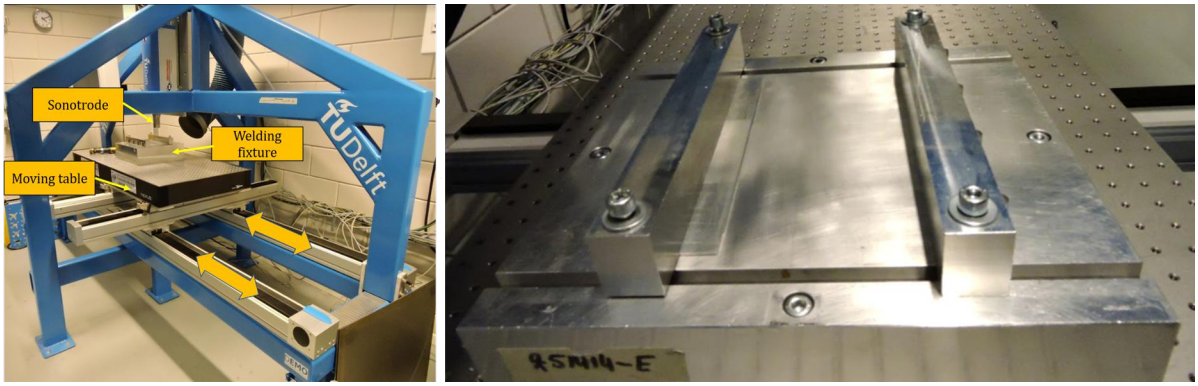

Figure 3.5: The CUW machine used for the making the continuous welds(left) and the fixture used to hold the specimens(right)

The fixture holds the substrates in place with the help of bar clamps, while being fixed to a table that moves at a constant speed. While the table is in motion, the sonotrode drops down and starts vibrating, hence creating a weld along the overlap of the plates. the maximum length of the plates that can be fixed into the fixture is 220mm. The speed of the table can be varied from 1mm/s to 100mm/s.

3.4. Optical Microscopy

The optical microscopy involved in this research was done mainly using two microscopes: a Leica optical microscope to do the cross-sectional microscopy and a Keyence VHX-2000 digital microscope for studying the deformations.

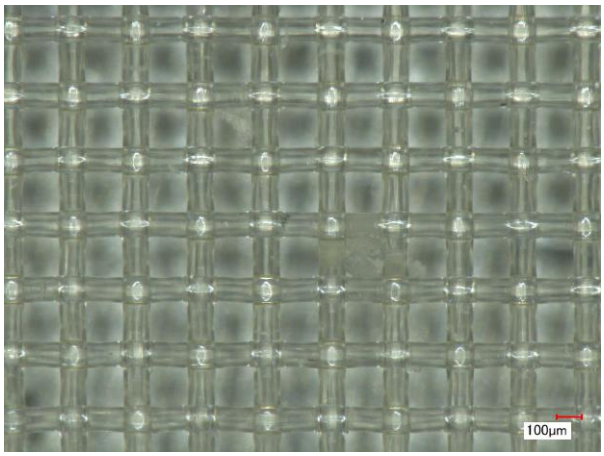

Figure 3.6: A sample image from the Keyence VHX-2000 microscope, showing the structure of a woven mesh

3.5. Mechanical Testing

The resulting joints have an overlap length of 12.7mm and are tested using a Zwick/Roell 250kN universal tensile testing machine with hydraulic grips and a loading rate of 1.3mm/min as per the ASTM 1002 D standard. In case of the CUWs, the specimens are cut into coupons of 25.4mm width to conform with the standard. The specimen dimensions are shown in Fig.3.8

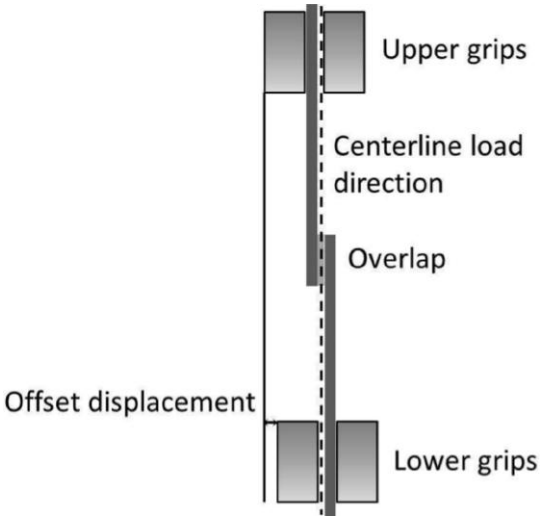

Figure 3.7: The setup of the specimen in the UTM for LSS testing

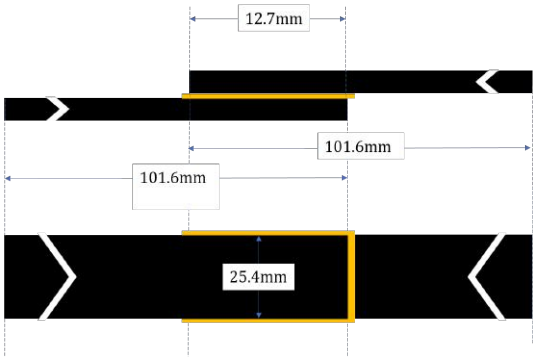

Figure 3.8: The dimensions of the specimens used for LSS testing

4

Manufacturing of energy directors

This chapter deals with the part of the research where different manufacturing options for the energy directors were explored. The objective of this part of the research was to manufacture an energy director that would satisfy the two requirements concluded from the literature survey: small contact points, an even spread of these contact points and some preforming.

4.1. Fused Deposition Modelling (FDM)

The first attempt to manufacture the energy director was done through FDM. The parameters mentioned in Table 4.1 were used for extruding the PEEK filament. The extrusion was done on PEEK foils of two thicknesses: 0.05mm and 0.5mm taped to the top of the build platform. The Z-offset of the printer was set in a way to make sure the nozzle did not touch the PEEK foil. The temperature of the nozzle was set to 400°C, which is higher than the melting temperature of PEEK (343°C), in order to ensure a smooth flow of the material.

Parameter	Setting
Build material	PEEK
Nozzle temperature [°C]	400
Build platform temperature [°C]	25
Extrusion width [mm]	0.4
Nozzle speed [mm/s]	130
Extrusion multiplier [-]	0.85

Table 4.1: The settings of the parameters used for printing

A simple design shown in Fig.4.1 which would theoretically offer some deformation prior to melting was chosen. The contact points were chosen to be toroidal in order to provide a large contact surface with a lower resin content and a lower extrusion time compared to a solid cylindrical contact point. As an approximation, the radius of the toroid was chosen to be twice that of the extruded thickness of 0.4mm to prevent overlapping of the deposited material, and the distance between the center of the toroids was set to 5mm.

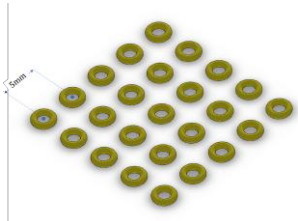

Figure 4.1: The geometry of the printed over the PEEK film on the bed

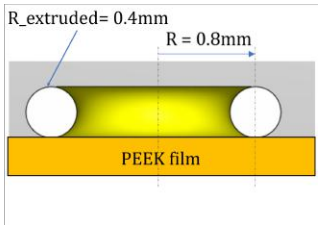

Figure 4.2: A cross-sectional view of the printed geometry

The extrusions were made on films of two thicknesses: 0.5mm and 0.05mm. The films were secured using a Kapton tape from all sides to prevent any movement of the film during the extrusion process. The build platform was not heated, and maintained at room temperature to avoid any warpage because of the heat.
On the film with a 0.05mm thickness, the heat from the nozzle caused a lot of warpage which led to the film coming in contact with the nozzle and hence causing it to stick. This resulted in a lot of holes in the film, and hence a poor quality energy director.
In case of the 0.5mm thick film, a lack of adhesion was noticed between the extruded PEEK and the PEEK film. This was probably due to the lower temperature of the build platform. An increase in the build platform temperature however caused warpage in the film, and the problems similar to those in the previous case were encountered. The end product of both the cases is shown in Fig.4.3 and Fig.4.4 respectively.
To overcome this problem, a more continuous extrusion solution was preferred: printing

Figure 4.3: PEEK extrusion on a 0.05mm thick PEEK film, with the build platform at room temperature

Figure 4.4: PEEK extrusion on a 0.5mm thick PEEK film, with the build platform at room temperature

continuous PEEK strips on top of the film in place of the toroids. Theoretically, this would provide better adhesion with the base film because of a larger contact area over the strip for every extrusion. Moreover, an extra offset to increase the distance between the nozzle and the build platform was set to 0.2mm in order to prevent any warpage from the heated nozzle. The end result is shown in Fig.4.5

Figure 4.5: Extruded PEEK strips on a 0.05 mm thick film

The extrusions showed much better adhesion to the base film, although a few holes and warpages were observed at some locations, the end product was more intact and usable as an energy director.
Cross-sectional microscopy was performed to have a closer look at the extruded geometry of the extruded PEEK on the PEEK film, as seen in Fig.4.6

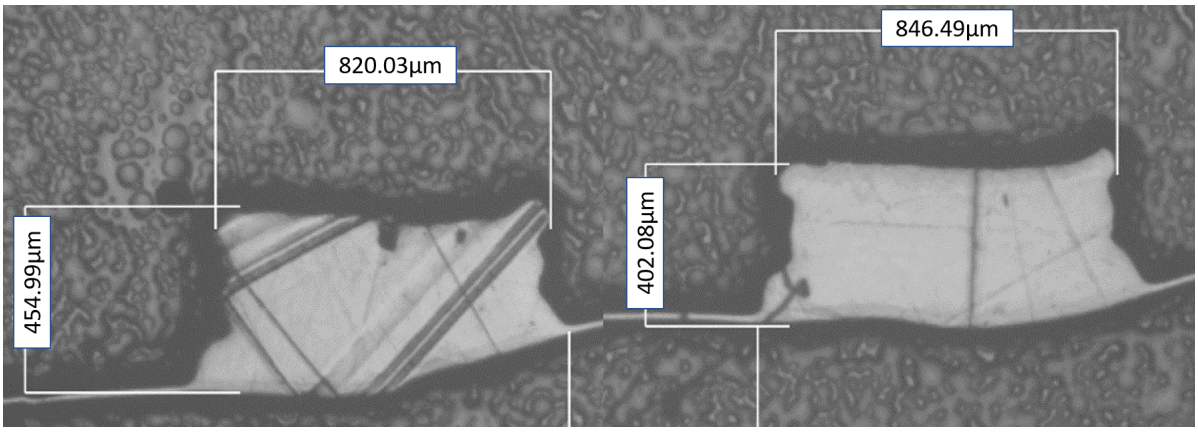

Figure 4.6: The dimensions of the extrusions made on the 0.08mm thick PEEK film.

It was observed that there was a difference of a maximum 15% in the thickness among the individual extruded PEEK strips.

4.2. Moulded energy directors

The next approach to manufacture the energy directors was through moulding PEEK films to have some conical protrusions. A conical shape was chosen to ease the removal of the ED from the mould. A conceptual design of the ED is shown in Fig.4.7 The moulds were

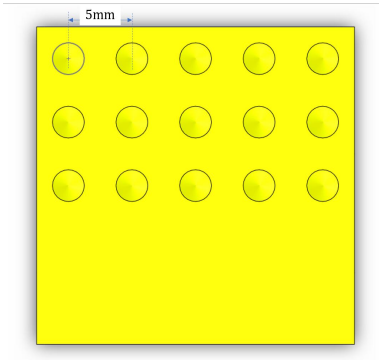

Figure 4.7: A top view of the 3-D model of the conical ED

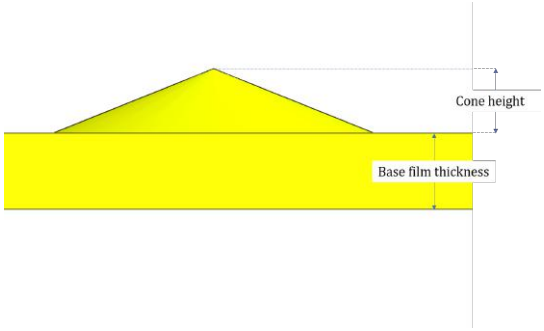

Figure 4.8: A side view of the 3-D model of the conical ED showing the dimensions

made on Aluminium sheets using a bench drill to make conical depressions, evenly spaced at every 5mm center to center. Although a bench drill is not the best solution for cases with such small dimensions such as this one, this part of the experiment was meant rather as a proof of concept for the mould. Three moulds with different cone depths were prepared to create a relation between the height of the cones and the preforming. The three different depths resulted in cone heights of 0.148mm. 0.266mm and 0.306mm respectively, with a constant base thickness of 0.12mm in all the cases when measured over 5 points using a screw gauge. The angles of the cones in the moulds were measured using the cross-section microscopic image of the cone as shown in Fig.4.11, and was found to be equal to the drill angle (135°).The energy directors were consolidated in a hot platen press as per the scheme shown in Table4.2 and Fig.4.9

	CF/PEEK	CF/PPS
Temperature [°C]	385	320
Consolidation Time [min]	10	10
Pressure [MPa]	2	2

Table 4.2: The processing parameters for manufacturing the conical energy directors

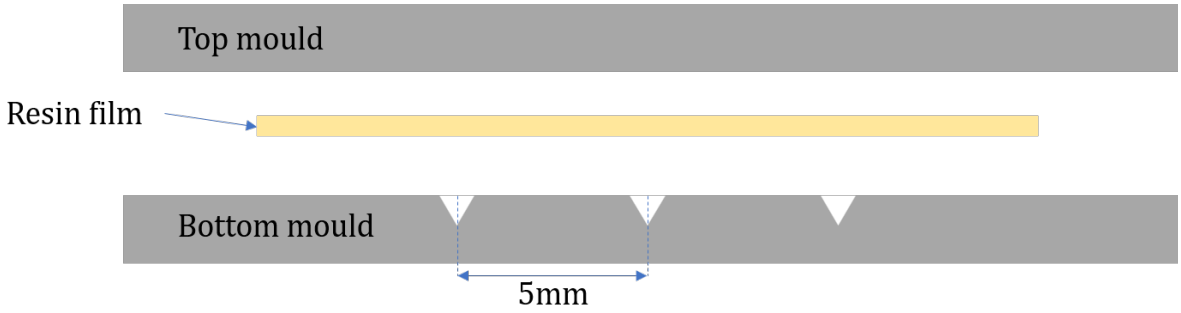

Figure 4.9: The layout of the moulding scheme used for the conical energy directors

The resulting energy director was structurally intact and had a uniform base thickness. However, due to the inaccuracies of the drilled depressions in the mould, the cones were not of a uniform height throughout and the geometry of the protrusions was rather spherical than conical. The non-uniformity in the cone heights was expected because of the human factor involved in the bench drill and the spherical geometry was attributed to the air trapped inside the depressions during the melting of the resin film. Nonetheless, this experiment served as a good proof of concept for the mould and the resulting energy directors were deemed worthy enough of providing a rough estimate of the behaviour of this design. The resulting ED is shown in Fig.4.10

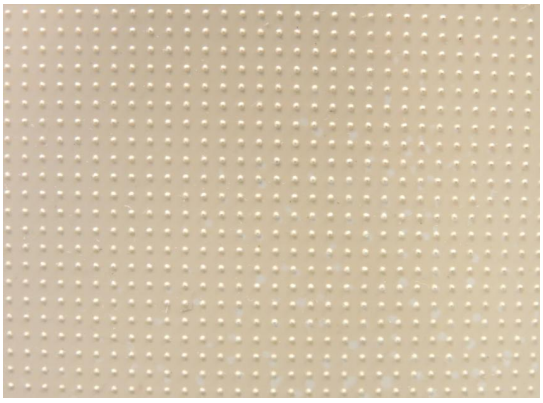

Figure 4.10: The conical ED manufactured through moulding

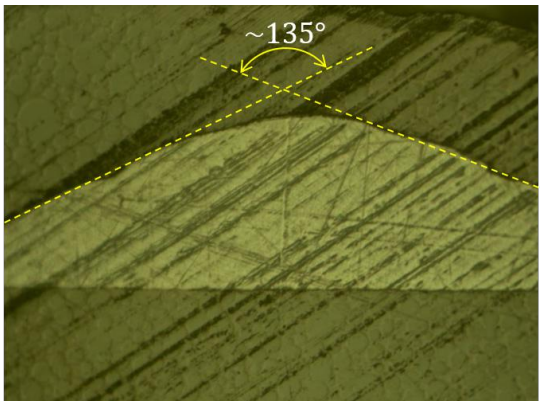

Figure 4.11: Cross-sectional image of this ED showing the angle of the cone

4.3. Conclusions

This part of the research was aimed at exploring different manufacturing methods for the energy directors that would help create an intimate and uniform contact between the substrates. Using FDM can be a bit tricky, given the high temperatures that causes warping in the thin PEEK film at the base. A thick PEEK film showed poor adhesion with the extruded PEEK and hence was not seen as a viable option. In order to use a thin sheet (0.08mm thick), the build platform temperature has to be kept as low as possible to prevent any warpage from the heat. These warpage can cause the film to come in contact with the nozzle of the 3-D printer. Moreover, it was observed that the heat from the nozzle also caused local warpage, which again caused the film to come in contact resulting in holes because of burning. To combat this problem, a simpler design with just strips was chosen. When printing strips, the nozzle does not remain at the same spot over the film for a long time, hence reducing the possibility of warpage. However, this problem could not be eradicated completely as at some parts of the film, the same problem was still observed.

In case of the conical energy directors, the manufactured EDs were seen to have a good structural integrity and uniformity in terms of the base thickness. The experiments showed promising results for manufacturing the EDs using moulding. However, since the conical depressions were done using a less accurate bench drill, the cone heights showed higher variations. To overcome this problem, a CNC controlled drill was used after evaluating other aspects of this design, which is explained in the next chapter.

5

Characterization of the energy directors through spot welds

In this chapter, four ED options were studied by using them for spot welds. The power-displacement curves from each of these ED options gives information about the location of the displacement plateau and the corresponding time and displacement value. The power-displacement curves also serve the purpose of identifying the optimum weld time for highest LSS value, as discussed in the literature review. Firstly, spot welds are performed on the four ED options under the same conditions to obtain their power-displacement data and important characteristics of these curves are studied in detail. This is then followed by determining their optimum LSS for use as a reference for CUWs.

5.1. Spot welding

Spot welds were used to determine whether the different energy directors showed a plateau in the displacement curves, and to find out the value at which they showed this plateau. For every ED option, 3 specimens were welded.

5.1.1. Woven mesh - PEEK

The power displacement curves when using a 0.20mm thick woven PEEK mesh as an ED are shown in Fig.5.1

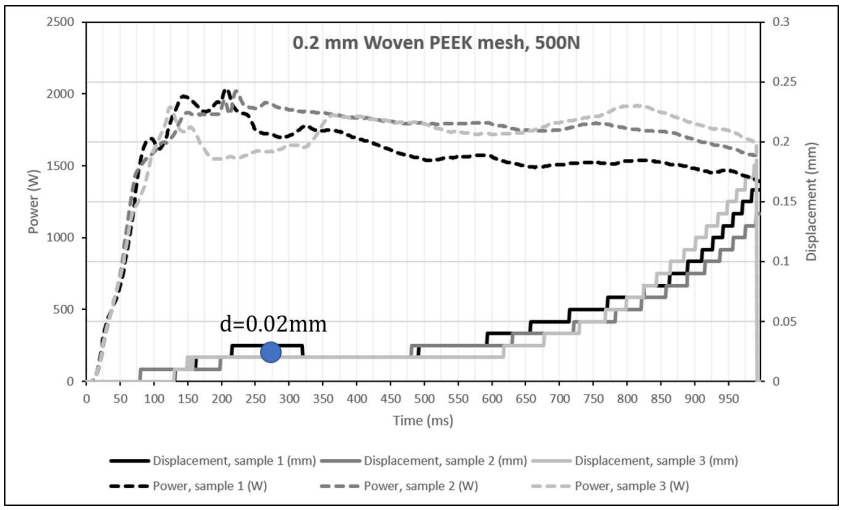

Figure 5.1: The power-displacement curve for the 3D-printed PEEK strips

The displacement plateau was observed at a depth of 0.02mm, and it was reached roughly 200ms into the welding process. This likely pre-forming is lower than what was observed by Jongbloed et al. when using a PPS mesh as an ED for CF/PPS laminates(d=0.065mm) and is reached comparatively slower (t=120ms)[10]. This is possibly due to the fact that PEEK has a higher glass-transition temperature(around 143°C) compared to PPS(around 85°C)[1], which means that PPS starts losing its modulus earlier compared to PEEK when the temperature at the interface is increasing.

5.1.2. FDM - PEEK Strips

The power-displacement curves when using 3-D extruded PEEK strips on 0.05mm thick PEEK film as an ED are shown in Fig.5.2

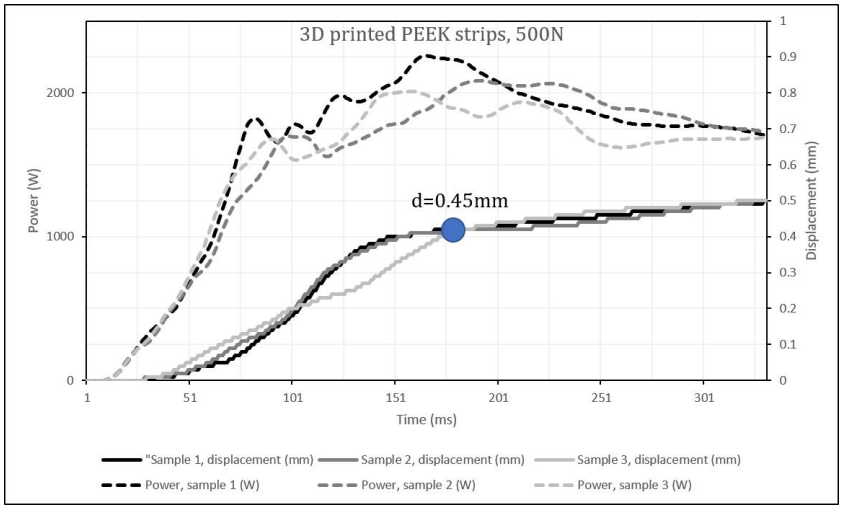

Figure 5.2: The power-displacement curve for the 3D-printed PEEK strips

The plateau was observed at a depth of 0.45mm, which is almost equal to the thickness of the extruded PEEK strips (roughly 0.44mm).
Although the the PEEK FDM ED showed the desirable plateau in the displacement curve, it was not considered for further research due to three reasons:

- The extruded filament from the printer had a minimum layer height of 0.25mm, which meant that the dimension of the strips can be modified only in multiples of 0.25, with 0.25mm being the minimum possible height. This limits the flexibility of the design when dealing with very small dimensions.
- Despite the fact that the extruded strips showed good adhesion to the film, there were a lot of inconsistencies in the final ED in terms of the base layer. Due to local warpages, the nozzle came in contact with the film, causing burnt areas with no resin under the strips. This brings in other factors into the play, which are out of scope of this study.
- Lastly, the 3-D printer available at DASML has a build volume of 140 x 135 x 148 mm which is not enough to create longer energy directors needed for the CUW welding.

Nevertheless, this part of the study acts as a proof of concept that FDM can be used to manufacture loose EDs using films as a base layer, and with more research this can be used as an effective tool to manufacture EDs with complex geometries.

5.1.3. Conical moulded ED - PPS

In case of the conical moulded energy directors, three cone heights were used to check if there was an empirical relation between the cone height and the preforming distance observed in the power-displacement curve. For clarity, the three heights are assigned an letter in relation to their sizes as follows:

Cone height(h_c)	Reference letter
0.148mm	S
0.266mm	M
0.414mm	L

Table 5.1: The cone heights tested in the ED to determine a relation between the cone height and preforming

An analytical approach was first taken to estimate the preforming of the cones assuming that the cones melt completely to form another layer of molten resin on top of the base film as shown in Fig.A.4.

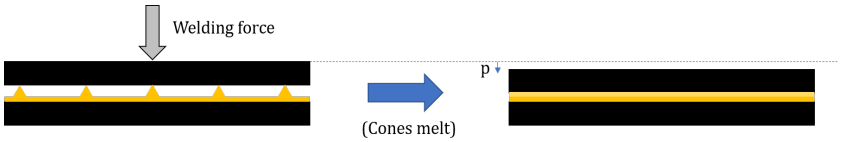

Figure 5.3: The power-displacement curve for the conical-S ED

For an overlap of 25.4mm x 12.7mm, the following equation was obtained(the derivation is showed in the appendix):

$$p = h_c - 0.017 * n * h_c^3 \tag{5.1}$$

With p = preforming distance; and h_c = height of the cone from the top surface of base film. The calculated values for S, M and L are summarised in Table5.2 The forthcoming welds using the S, M and L EDs were performed to validate this equation. The power displacement curves and the preforming depth are shown in Fig.5.4, Fig.5.5 and Fig.5.6 respectively.

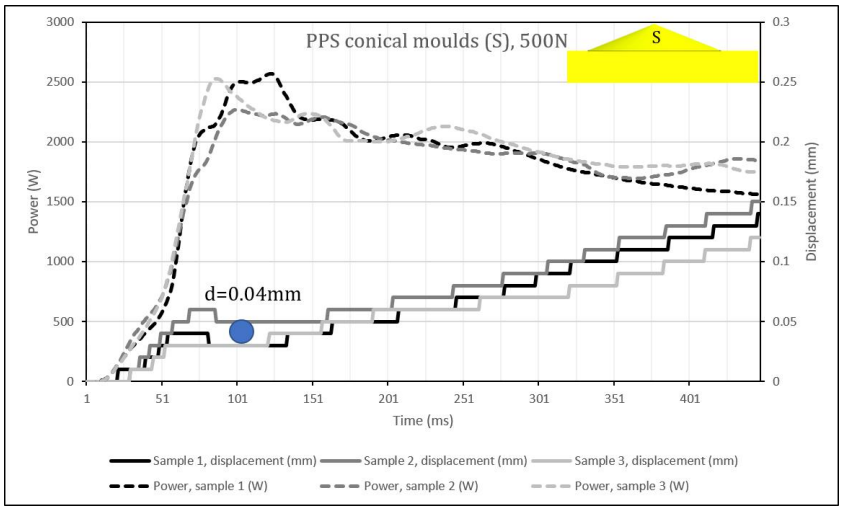

Figure 5.4: The power-displacement curve for the conical-S ED

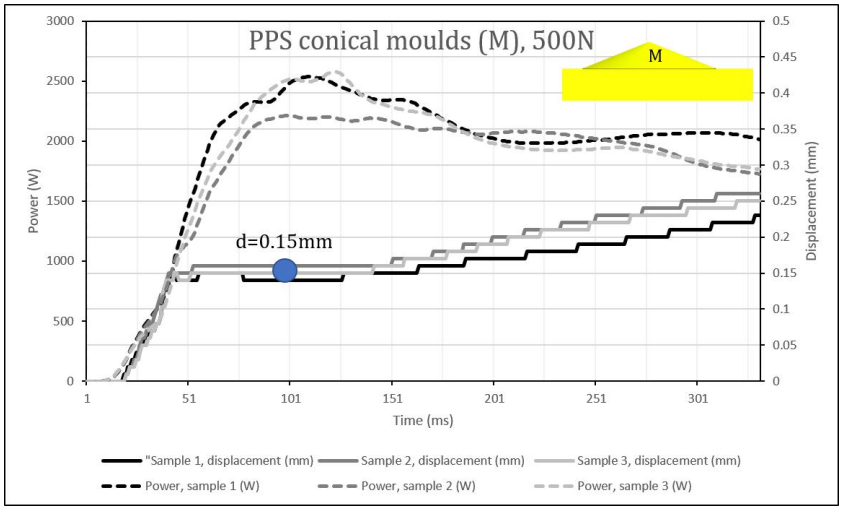

Figure 5.5: The power-displacement curve for the conical-M ED

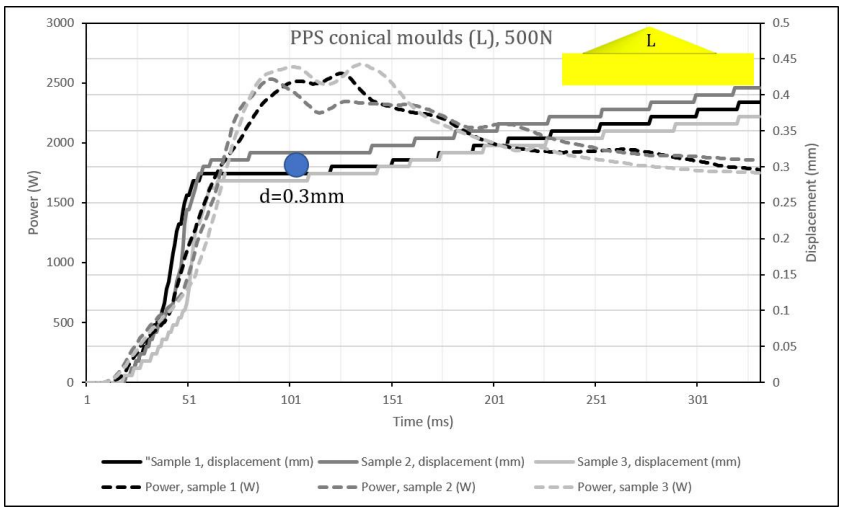

Figure 5.6: The power-displacement curve for the conical-L ED

The pre-forming distances are summarised in table 5.2.

Cone height(h_c)	Calculated pre-forming	Observed pre-forming
0.148mm (S)	0.147 [mm]	0.04 [mm]
0.266mm (M)	0.263[mm]	0.15 [mm]
0.414mm (L)	0.41[mm]	0.3 [mm]

Table 5.2: The cone heights and their corresponding pre-forming distances

It was observed that the data from the experiments did not fit into the equation derived analytically (Equation 5.1). To investigate this, the welding process was first stopped at three points when welding a size 'S' ED as shown in Fig.5.7

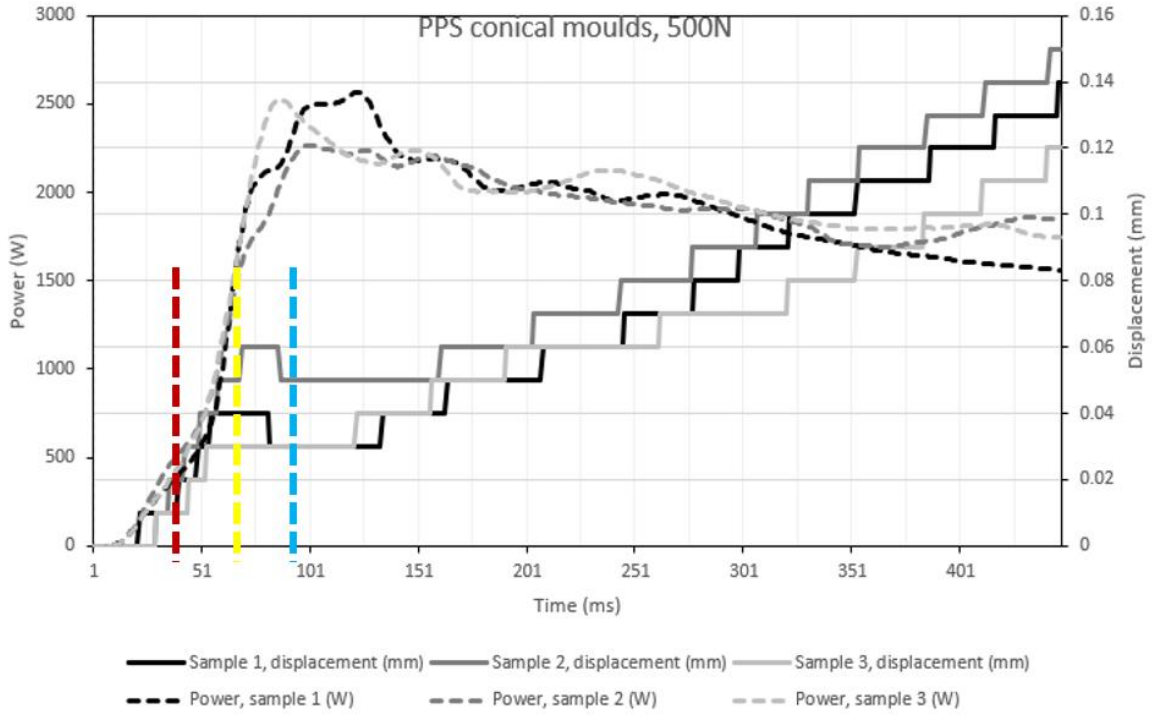

Figure 5.7: The welding process was stopped at welding time of 45ms, 70ms and 90ms to study the interface

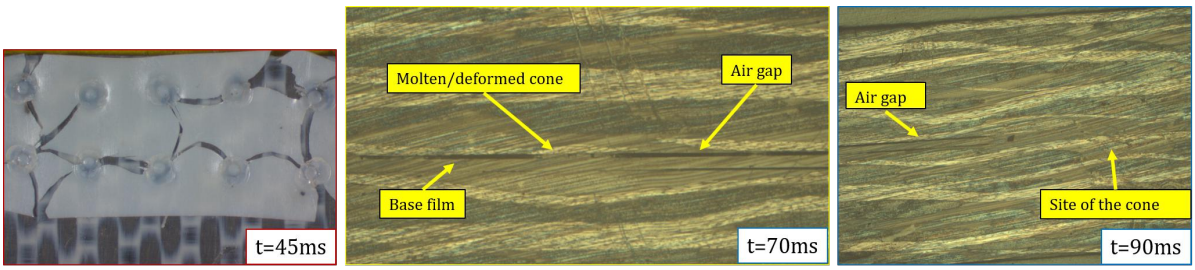

Figure 5.8: The interface at the corresponding weld times

From the images shown in Fig.5.8 it was could be seen that the cones do not melt completely to form a layer of molten resin on top of the base layer. The cones melt locally and the molten resin from adjacent cones do not meet to create a uniform layer, resulting in air gaps between them.

Hence, a trend line was generated from the experimental results to establish a relationship between the height of the cones and its corresponding preforming, as shown in Fig.5.9.

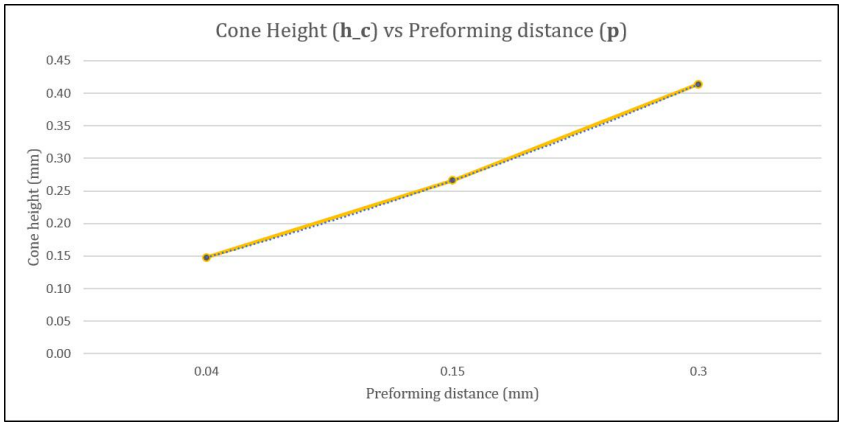

Figure 5.9: Cone height vs the pre-forming from the experiments

Using curve-fitting technique, the linear relation between the height of the cones and the pre-forming is shown in equation 5.2:

$$h_c = 1.021p + 0.109 \tag{5.2}$$

This equation can be useful in determining the cone height that is needed to reach a certain amount of preforming when using this ED. It is important to note that this equation only considers 10 cones, 5mm apart at the interface on 0.12mm thick base, and it only applies for PPS EDs since PEEK EDs were not used in this set of experiments.
The motivation behind deriving this relation was to manufacture a conical ED that would have the same preforming as that of the PPS mesh used in prior research[10], which is 0.065mm under similar conditions. In order to achieve this preforming through the conical ED made of PPS, the height of the cones as per equation5.2 should be 0.17mm. The next part describes how automated manufacturing techniques are used to manufacture a precise version of the conical ED.

5.1.4. Precision controlled conical energy directors - PEEK

Once the relation between the cone height had been determined, a 3-D model of the mould was created. The depth of the conical depression in the mould was set to 0.19mm, after giving an allowance for the air pocket that gets created. The mould was then manufactured using a CNC drilling machine at the DASML to have a consistent cone height. To gather more data about the EDs behaviour, two options were evaluated, as shown in Fig.5.11. The two ED options are herafter referred to as Con2.5(Cones 2.5mm apart) and Con5(Cones 5mm apart).

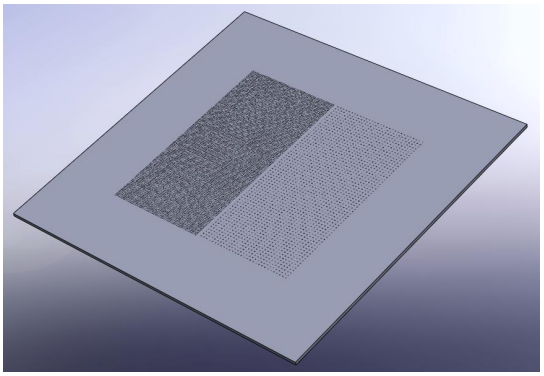

Figure 5.10: The 3-D model of the mould that was converted into a STEP file for manufacturing

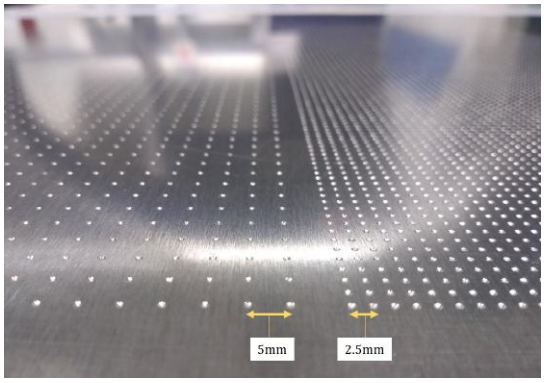

Figure 5.11: The manufactured mould with the two distinct sections of Con5 and Con2.5

The resulting ED from this mould however showed a higher cone height than the intended value. The heights of the cones were observed to be approximately 0.21mm, instead of 0.19mm. This was possibly due to the thermal expansion of the aluminium(between 21-24 x 10^{-6} /K [7]) mould at the higher temperature, which was not taken into account during the design.

Switching to conical PEEK ED from PPS:

The decision to use a conical PPS ED was driven by the existence of PPS CUW data from prior research. However, with the deviation from the intended design of the conical ED and the introduction of a PEEK expanded mesh midway through the scope of the research was shifted an all-PEEK ED comparison instead of an all-PPS comparison.

The mould however, was not remade because of the time and effort involved. The same mould was used to manufacture PEEK EDs and it was evaluated and characterized through spot welds. The resulting PEEK EDs showed a consistent cone height of roughly 0.2mm and a base height of around 0.1mm, resulting in a total ED height of approximately 0.3mm from the bottom side to the tip of the cone. These measurements were made using a screw gauge over the corners of the ED, as mentioned in Chapter 3.

The power-displacement behaviour of Con5 is shown in Fig.5.12 and of Con2.5 is shown in Fig.5.13

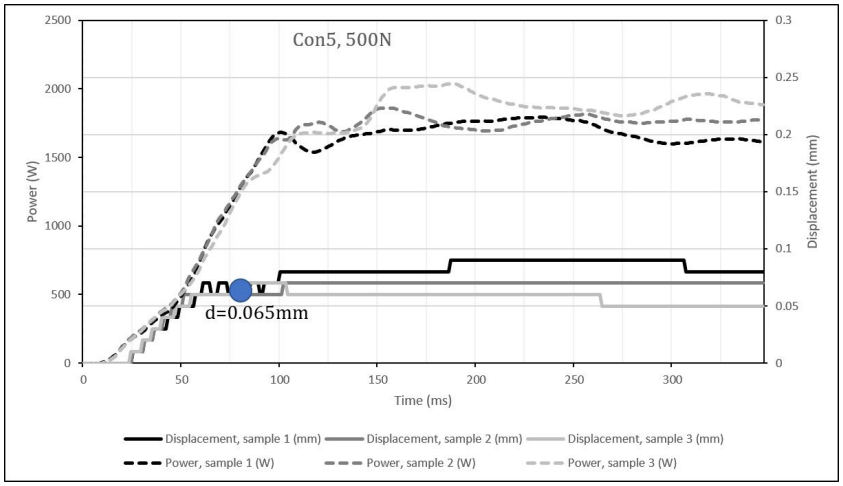

Figure 5.12: The power-displacement curve for the Con5 ED

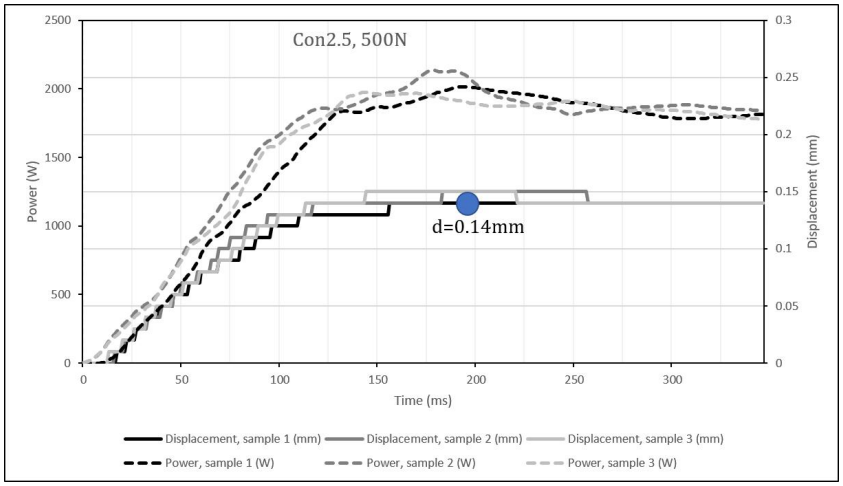

Figure 5.13: The power-displacement curve for the Con2.5 ED

The displacement plateau was observed roughly at a depth of 0.065mm in case of the Con5 ED and at a depth of 0.14mm in case of the Con2.5 ED.
To understand the difference in the pre-forming depth between Con5 and Con2.5, cross-sectional microscopy was performed at different points along the displacement curve. In case of the Con5, the welding was stopped just before the plateau was reached, at 60ms. The analogous spot for Con2.5 was at 75ms. The cones prior to deformation are shown as a reference in Fig.5.14 and the deformed cones are shown in Fig.5.15.

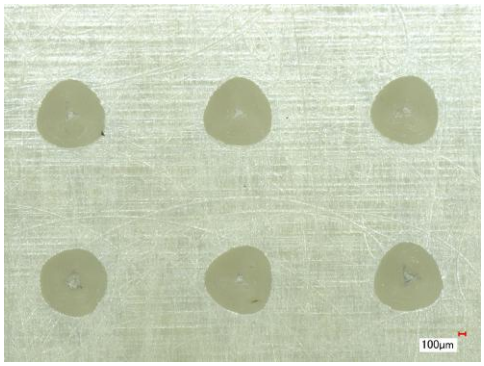

Figure 5.14: The surface of the ED (Con2.5) prior to the welding process

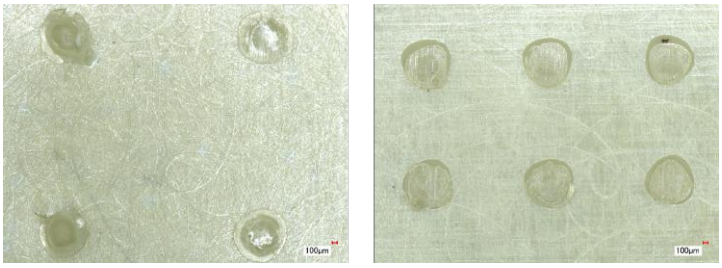

Figure 5.15: The surface of the Con5 ED at t=60ms (left) and Con2.5 at t=75ms (right)

The main observation among the two cases is the melting of the cones that is seen in the case of Con5 and is absent in Con2.5. The displacement plateau observed in the Con5 case seems to be a result of melting of the cones, whereas the preforming in the case of Con2.5 seems to be a result of the plastic deformation of the cones. This could likely be because of the fact that the force from the sonotrode is distributed among a comparatively lesser number of cones in the Con5 case.
To gain a better understanding of this ED, the welds were stopped a bit further into the displacement plateau: 130ms into the welding of the Con5 ED and 140ms into the welding of the Con2.5 ED. The resulting cross-sections are shown in Fig.5.16.

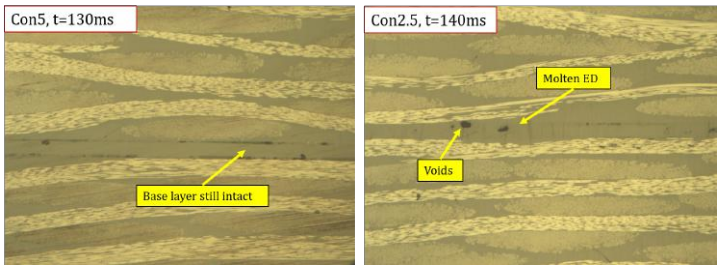

Figure 5.16: The cross-section of the Con5 ED at t=130ms (left) and Con2.5 at t=140ms (right)

Although the ED surface prior to the displacement plateau showed some melting in case of the Con5, this melting process doesn't seem to have reached the base film of the ED effectively. Whereas the Con2.5 case showed comparatively better melting of the ED, with bondline less visible. This is likely because of a higher number heat generation points in the Con2.5 ED, which transmits the melting process to the base film more uniformly. This probably results in a quicker melting process, once it has been initiated in the cones.

5.1.5. Expanded mesh - PEEK

An expanded mesh was also evaluated as an energy director option because of its similarity to a thin film while having open areas like woven meshes. The power-displacement curve for this is shown in Fig.5.17 The displacement curve showed two plateaus: one after roughly 30ms

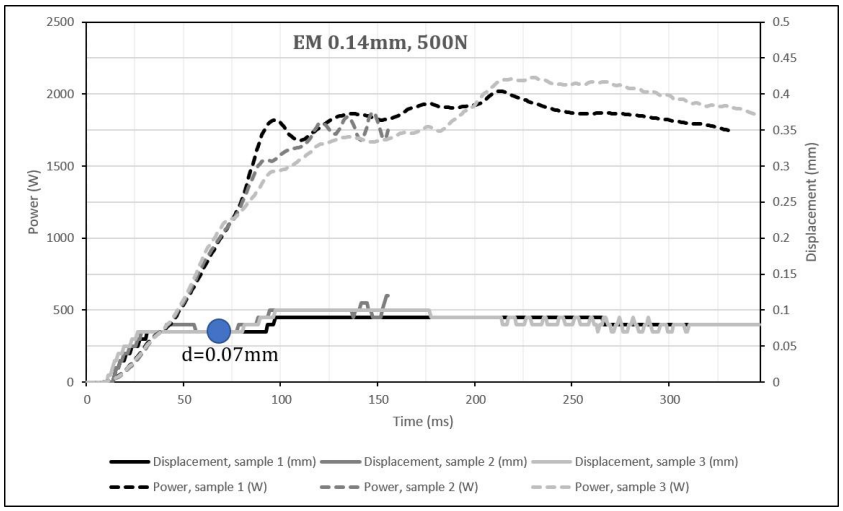

Figure 5.17: The power-displacement curve for the 0.14mm thick expanded PEEK mesh

and the other one after around 100ms. The second displacement peak coincided with a peak in the power peak as well, indicating a possible melting occurring at the interface. In order to better understand this, the welds were stopped along different points in the displacement curve: after 50ms of weld and 110ms of weld. The status of the interface at these time points are shown in Fig.5.18

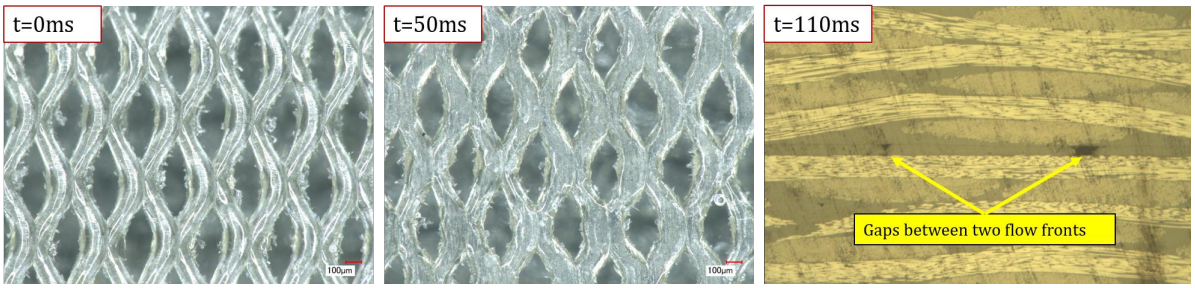

Figure 5.18: The progression of the ED over the weld time

Through these images, it was observed that at the first plateau the ED only showed deformation and negligible melting since the two substrates could be separated easily by hand. At the second plateau, however, there was some melting as the joint showed some strength. Some portions of the interface showed completely filled overlap while the others, as shown in Fig.5.18 showed some gaps which were likely closing in because of the molten flow of resin.

5.2. Lap Shear Strengths

From the power-displacement graphs of the EDs, the optimum weld time is noted down for each ED. Experience with using PPS woven meshes as EDs has indicated that the weld time for meshes is right at the end of the plateau, where the displacement starts increasing. Since expanded meshes and conical EDs have not been used before, it is assumed that the same trend follows for these as well. Hence, the same method is used to determine the optimum time for the highest possible LSS for each ED type. The assumed optimum weld times found from the power-displacement graphs are shown in Table 5.3. Three welds were performed for each type of ED to attain the average LSS.

	Assumed optimum weld time	Mean LSS
Woven mesh	500ms	40.23±1.85 MPa
Expanded mesh	400ms	36.75±3.18MPa
Conical 5mm	400ms	28.37±2.2MPa
Conical 2.5mm	500ms	38.43±2.27 MPa

Table 5.3: The optimum weld time and LSS values

It was observed that while the LSS of the woven mesh, expanded mesh and the Con2.5 were in a comparable range, the LSS of the Con5 ED was lower by roughly 10MPa.

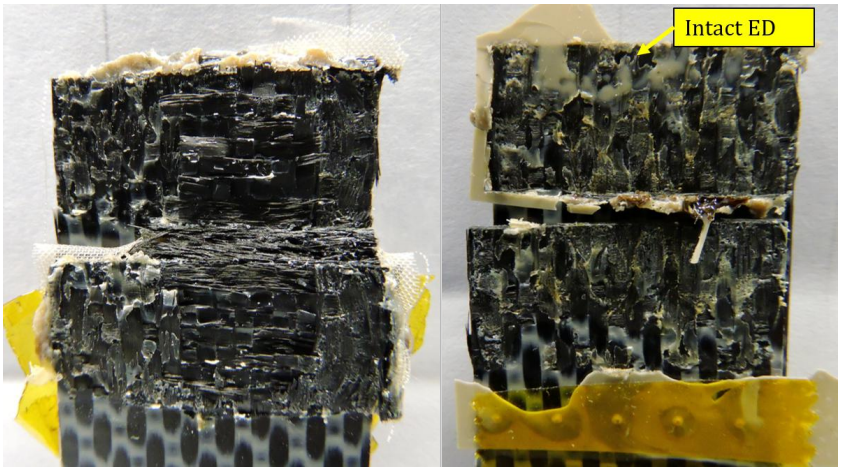

Figure 5.19: A comparison of the fracture surface of a Woven PEEK ED at the interface (left) vs Con5(right)

Fig.5.19 compares the fracture surfaces of weld using woven mesh ED with a Con5 ED, as they represent the highest and the lowest LSS respectively. The fracture surface of the Con5 specimen shows unwelded areas with a lot of intact resin at the interface. This is probably due to insufficient heat generated at the interface, indicating that probably a longer weld time is needed for this ED.

5.3. Conclusions

In this chapter, four types of EDs were evaluated: a woven mesh, extruded strips on a film, conical moulded and an expanded mesh. It was observed that the a PEEK woven mesh offered a lower pre-forming value compared to a PPS mesh of the same dimensions, probably due to the comparatively higher stiffness of PEEK at high temperatures. The extruded PEEK strip ED was used for spot welds, but was later discarded as an option for CUW because of poor quality and the limitations of the extruding machine. Conical EDs were successfully manufactured and an analytical relation was derived between the height of the cones and the preforming. A CNC machine was used to manufacture an accurate version of the mould with two variants in the same mould: Con5 and Con2.5. These two options were manufactured with PEEK and used for studying the features of this design. The final ED option was an expanded PEEK mesh that showed some preforming prior to the welding.

The next chapter deals with the CUW of the EDs evaluated in this chapter and analyzed to find a link between the data generated in this section and the results observed in the next part.

6

Behaviour of the energy directors in continuous ultrasonic welding

In this part of the research, the 4 ED options are used for CUW of CF/PEEK laminates. It is known through the literature [10] that for PPS mesh EDs, welding speeds of 45mm/s resulted in a uniform weld line. Since PEEK has a higher melting temperature, lower welding speeds of 25mm/s and 30mm/s were tried using the expanded mesh ED on smaller laminates of 101.6mm length and tested see whether the ED was melting. The fracture surfaces are shown in the Appendix section of the report. These results are not used for evaluation, as smaller welds do not give a lot of information about the true nature of the ED. Based on the observations, three welding speeds were chosen: 15mm/s; 20mm/s and 25mm/s for the comparisons.
First it is perhaps important to mention that the welds for all the speeds showed some delaminations in the side in contact with the sonotrode. This was independent of the type of the energy director being used. Fig.6.1 shows the top and bottom view of an example case.

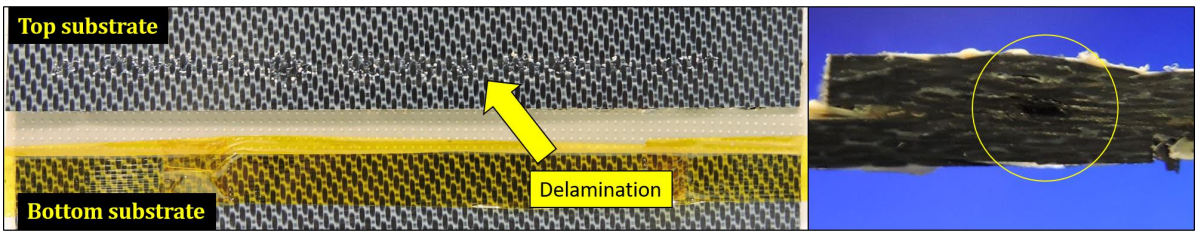

Figure 6.1: The top view of the delamination when using a conical ED at a welding speed of 20mm/s(left), and the cross-sectional view of the same with the delaminated portion in the circle (right)

This could possibly have an effect on the failure mode of the joint, when the joint fails along the delaminated region instead of the bondline. But since this delamination was common for all the cases, the forthcoming results produce a comparison with this defect present in all of them.

6.1. Results

6.1.1. Woven mesh - PEEK

Fig.6.2, Fig.6.3 and Fig.6.4 show the fracture surfaces of the 220mm long laminates welded at 15mm/s, 20mm/s and 25mm/s with a 0.2mm thick PEEK woven mesh as an ED. The corresponding LSS values are shown above each specimen.

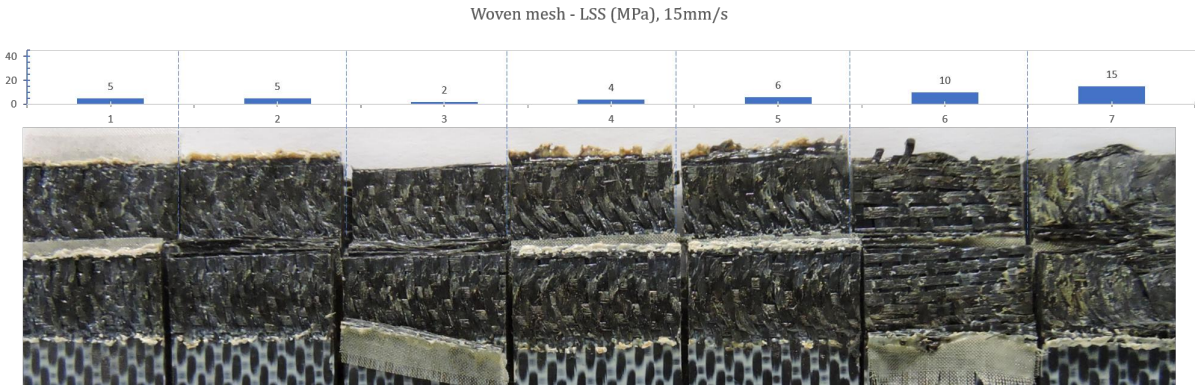

Figure 6.2: The fracture surfaces at a welding speed of 15mm/s

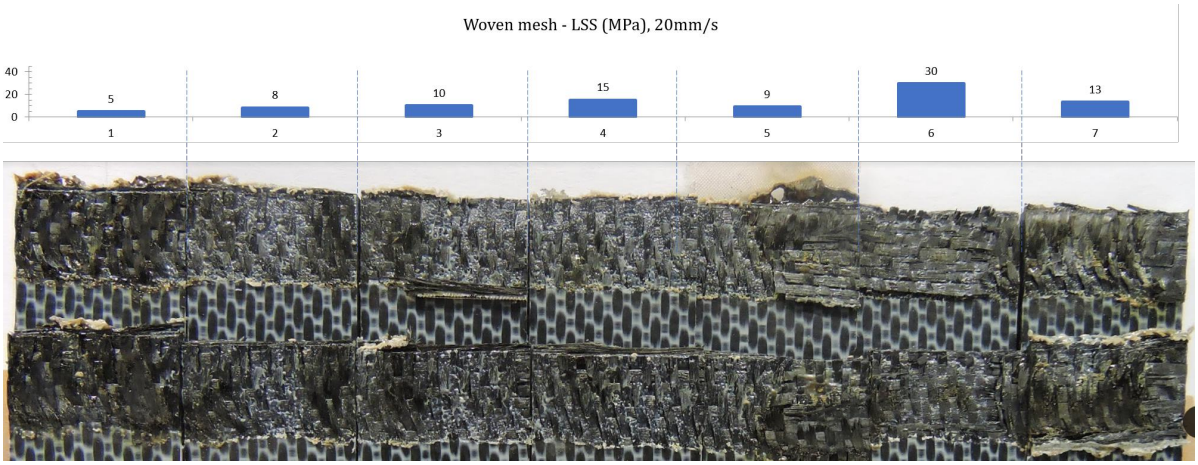

Figure 6.3: The fracture surfaces at a welding speed of 20mm/s

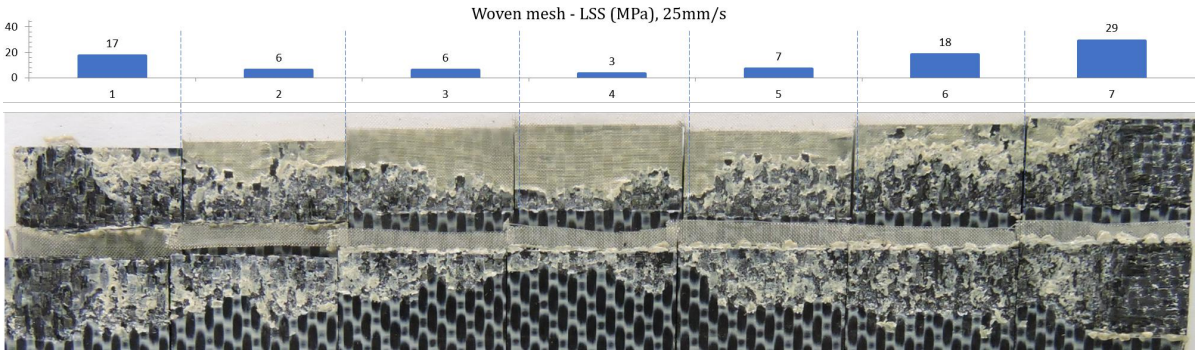

Figure 6.4: The fracture surfaces at a welding speed of 25mm/s

The single lap shear strengths of the woven mesh ED after discarding the edge specimens (n=7) are shown in Fig.6.5 and Table6.1

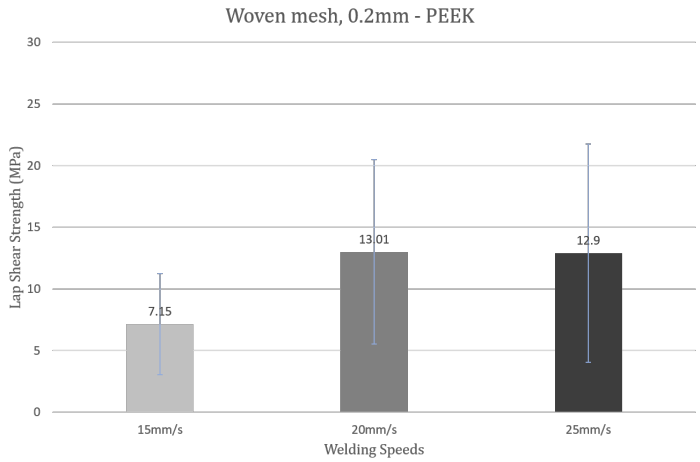

Figure 6.5: LSS of the 0.2mm thick woven PEEK ED

Welding Speed	Lap Shear Strength
15 [mm/s]	7.15 ±4.15 [MPa]
20 [mm/s]	13.01 ±7.48 [MPa]
25 [mm/s]	12.9 ±8.87 [MPa]

Table 6.1: The lap shear strengths of the CUW specimens with a PEEK Woven mesh as an ED

The primary observation at the speed of 15mm/s is the severe overheating of the interface which is visible in the form of burnt areas where the surface shows dark spots when it is moved under a light source. Due to overheating, the resin starts to burn, getting darker and in extreme cases it starts to evaporate from the surface, leaving just dry fibers behind. This is shown in Fig.6.6.

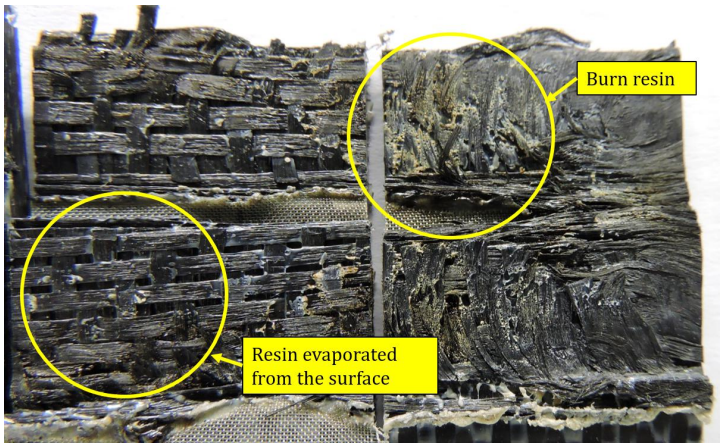

Figure 6.6: The overheating at the interface when using a Woven mesh

The burnt areas are also observed in the specimens welded at 20mm/s. However, at a speed of 25mm/s there is a lot of intact ED, which is an indication of poor heat generation at the interface.
The LSS of the specimens consistently showed a deviation of 50% across the three welding speeds.

6.1.2. Expanded mesh - PEEK

Fig.6.7, Fig.6.8 and Fig.6.9 show the fracture surfaces of the 220mm long laminates welded at 15mm/s, 20mm/s and 25mm/s with a 0.14mm thick PEEK expanded mesh as an ED. The corresponding LSS values are shown above each specimen.

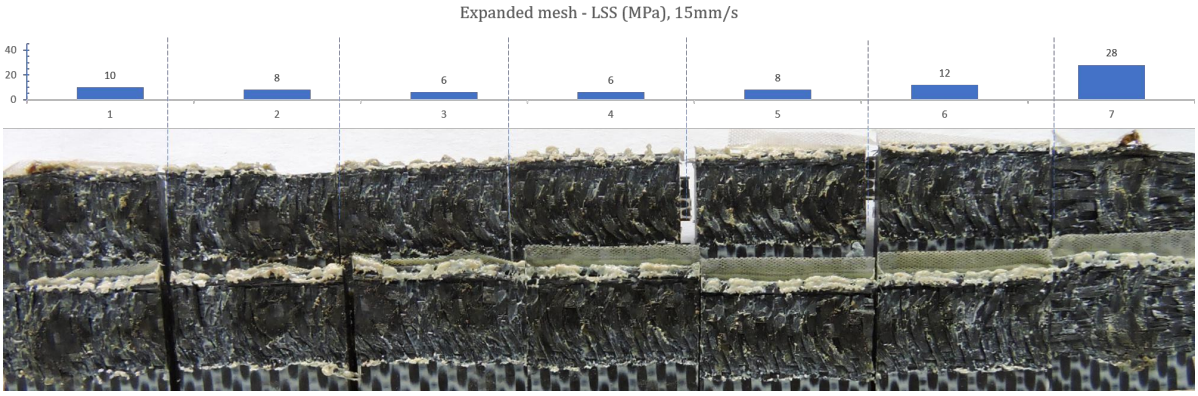

Figure 6.7: The fracture surfaces at a welding speed of 15mm/s

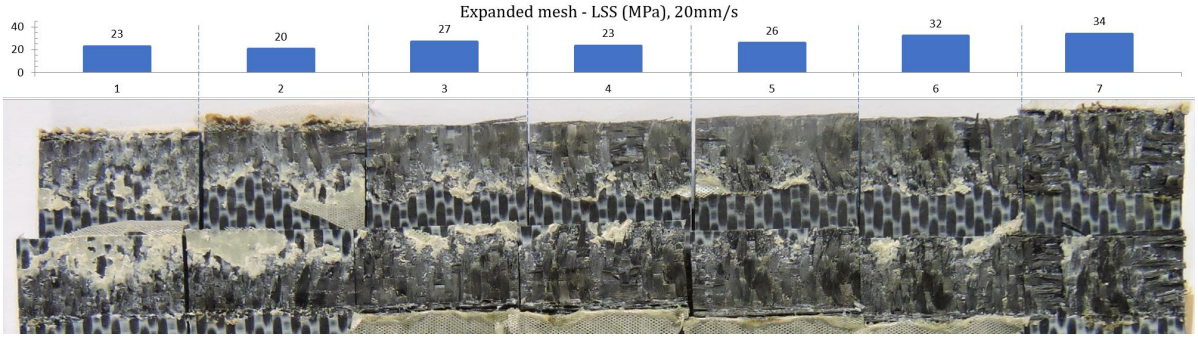

Figure 6.8: The fracture surfaces at a welding speed of 20mm/s

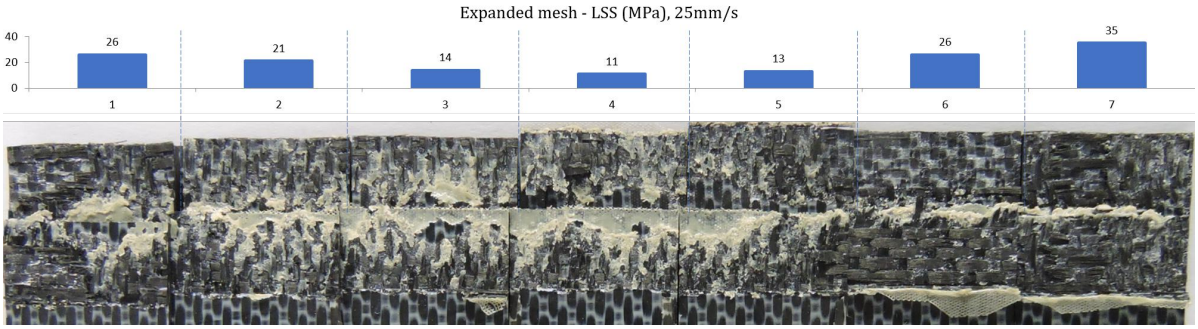

Figure 6.9: The fracture surfaces at a welding speed of 25mm/s

The single lap shear strengths of the expanded mesh ED after discarding the edge specimens (n=7) are shown in Fig.6.10 and Table6.2

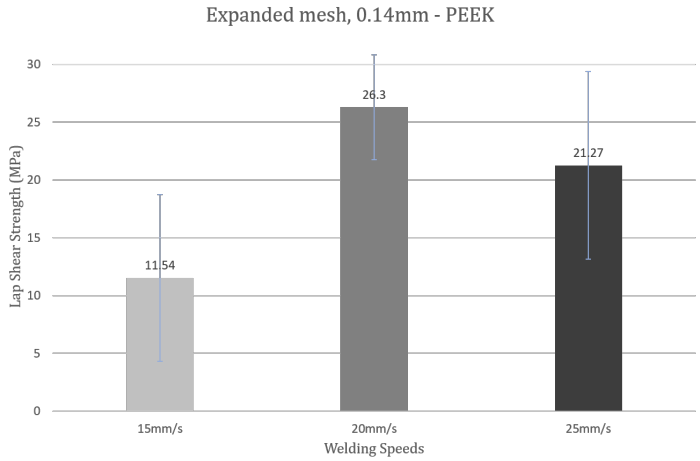

Figure 6.10: LSS of the 0.14mm thick expanded PEEK mesh ED

Welding Speed	Lap Shear Strength
15 [mm/s]	11.54 ±7.2 [MPa]
20 [mm/s]	26.3 ±4.54 [MPa]
25 [mm/s]	21.27 ±8.13 [MPa]

Table 6.2: The lap shear strengths of the CUW specimens with a PEEK expanded mesh as an ED

Similar to the case of the woven mesh, the expanded mesh also showed overheating at the interface which was visible in the form of burn marks. However, at a welding speed of 20mm/s some of the specimens showed a uniform heat generation, which is characterized by an even melting and spreading of the resin across the overlap. A closer view of the fracture surface that shows this phenomenon is shown in Fig.6.11

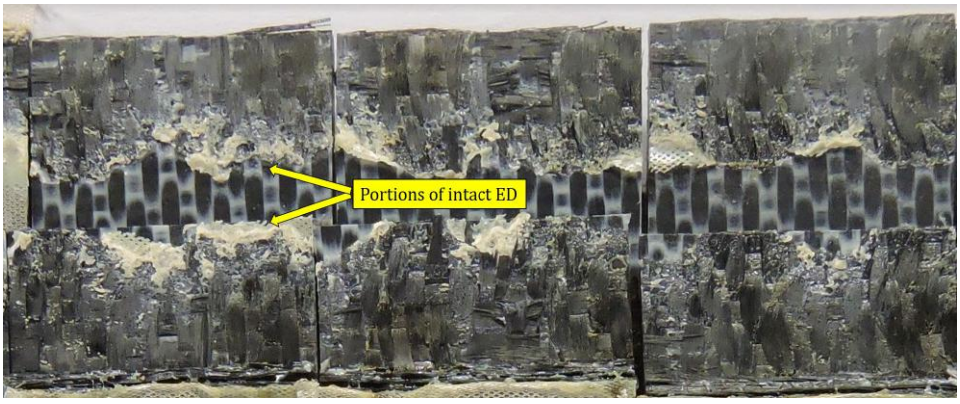

Figure 6.11: The fracture surfaces of specimens with an expanded mesh ED welded at a speed of 20mm/s that show a uniform heat generation. There are still some small portions of intact ED at the interface.

At a speed of 25mm/s however, there is a lot of intact resin left at the interface, which is an indication of insufficient heat generation.
The LSS strengths are in line with the weld quality observed at the interface, with the 20mm/s showing the highest value along with a comparatively lower value of scatter.

6.1.3. Conical moulded ED Con5 - PEEK

Fig.6.12, Fig.6.13 and Fig.6.14 show the fracture surfaces of the 220mm long laminates welded at 15mm/s, 20mm/s and 25mm/s with a Con5 PEEK ED. The corresponding LSS values are shown above each specimen.

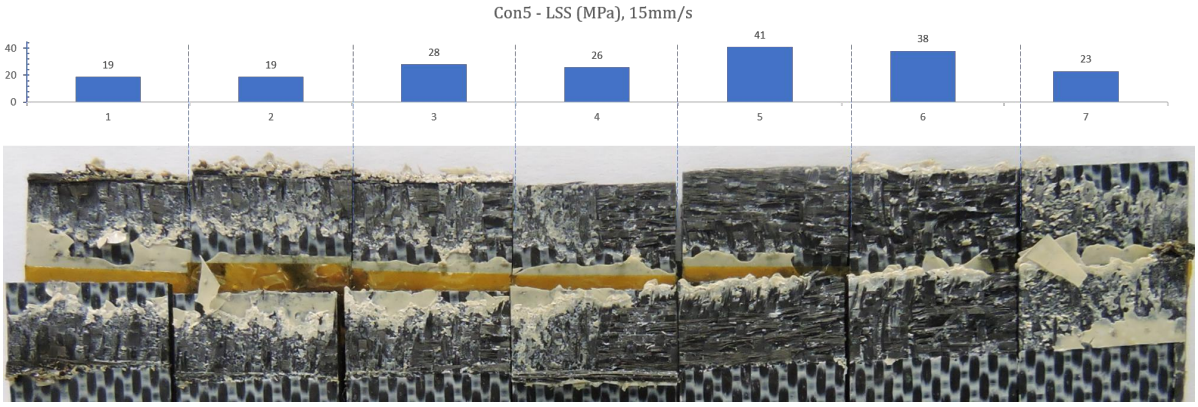

Figure 6.12: The fracture surfaces at a welding speed of 15mm/s

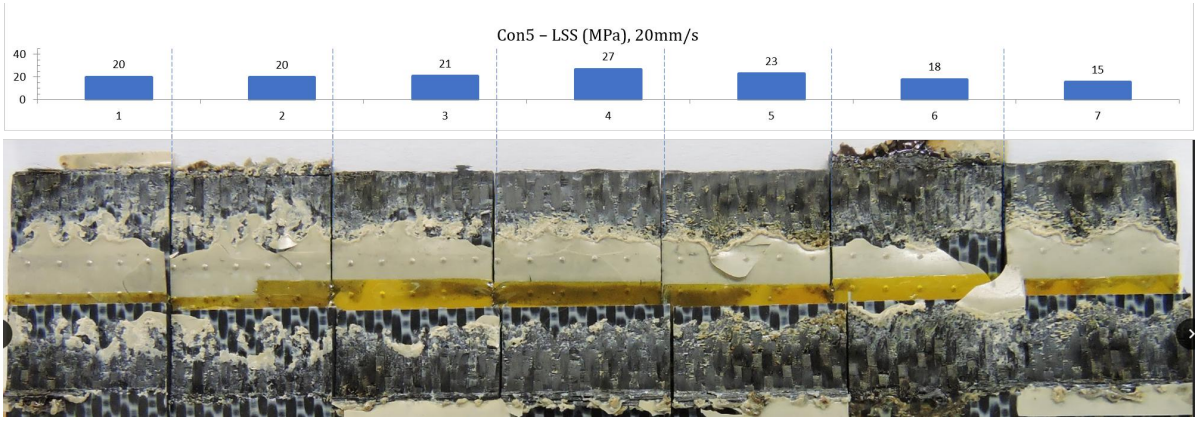

Figure 6.13: The fracture surfaces at a welding speed of 20mm/s

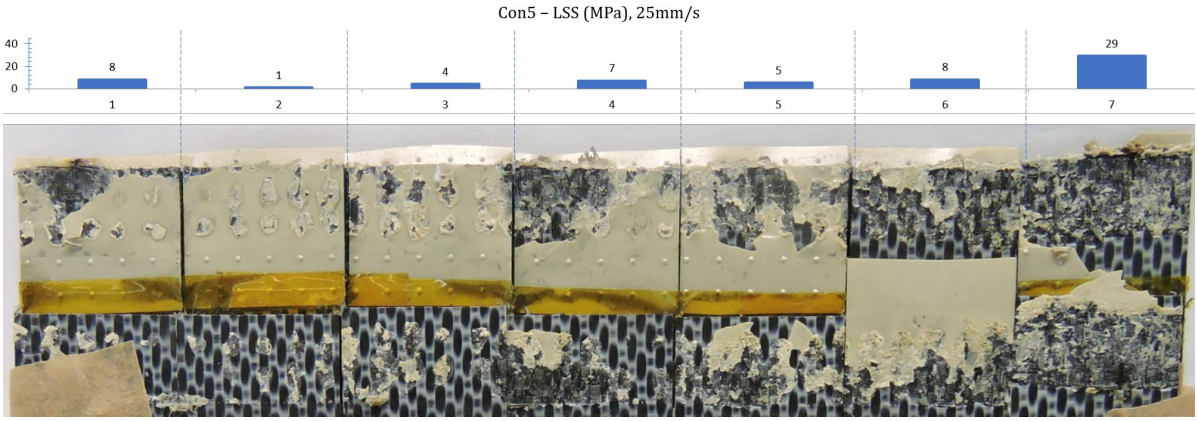

Figure 6.14: The fracture surfaces at a welding speed of 25mm/s

The single lap shear strengths of the Con5 ED after discarding the edge specimens (n=7) are shown in Fig.6.15 and Table6.3

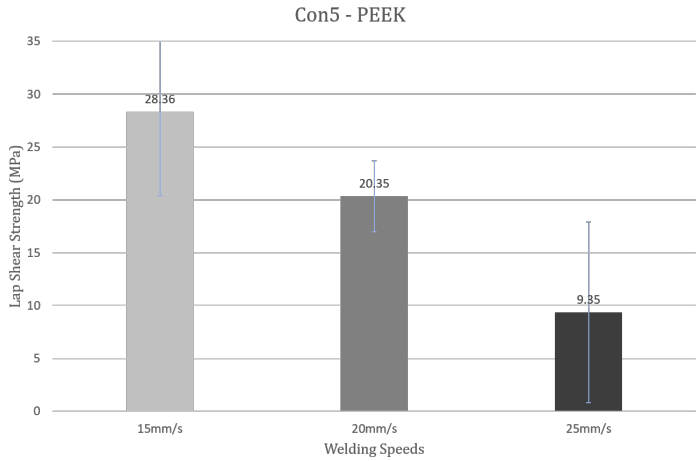

Figure 6.15: LSS of the Con5 PEEK ED

Welding Speed	Lap Shear Strength
15 [mm/s]	28.36 ±7.94 [MPa]
20 [mm/s]	20.35 ±3.36 [MPa]
25 [mm/s]	9.35 ±8.55 [MPa]

Table 6.3: The lap shear strengths of the CUW specimens with a Con5 ED

At a speed of 15mm/s, the Con5 ED showed a uniform heat generation and resin flow at the interface barring the end specimens. There was one burnt area observed at the start of the weld line and some intact resin at the end of the weld line.
At 20mm/s, although the overall resin uniformity over the surface looked positive, the heat generation towards the edge of the overlap looked insufficient to melt the ED in that region. An example of this is shown in Fig.6.16

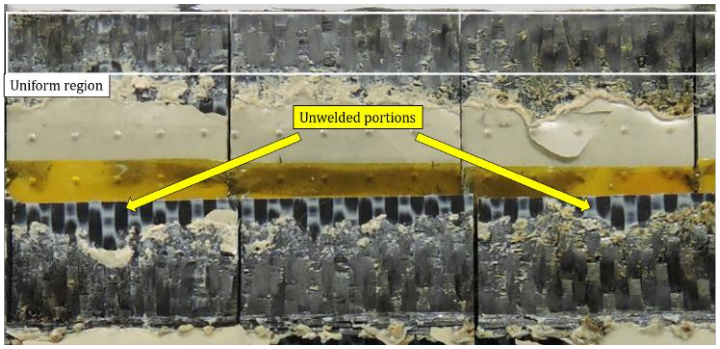

Figure 6.16: Fracture surface of the Con5 PEEK ED

When welded at a speed of 25mm/s. the EDs were found to be largely intact overall with some melting observed at just the cones, with the base film almost completely intact.
The LSS values were the highest at a welding speed of 15mm/s, while the values showed the lowest scatter at a speed of 20mm/s. At 15mm/s the LSS values were found to be the lowest, with only the last specimen offering a value in double digits. The scatter at this speed was close to a 100%.

6.1.4. Conical moulded ED Con2.5 - PEEK

Fig.6.17, Fig.6.18 and Fig.6.19 show the fracture surfaces of the 220mm long laminates welded at 15mm/s, 20mm/s and 25mm/s with a Con2.5 PEEK ED. The corresponding LSS values are shown above each specimen.

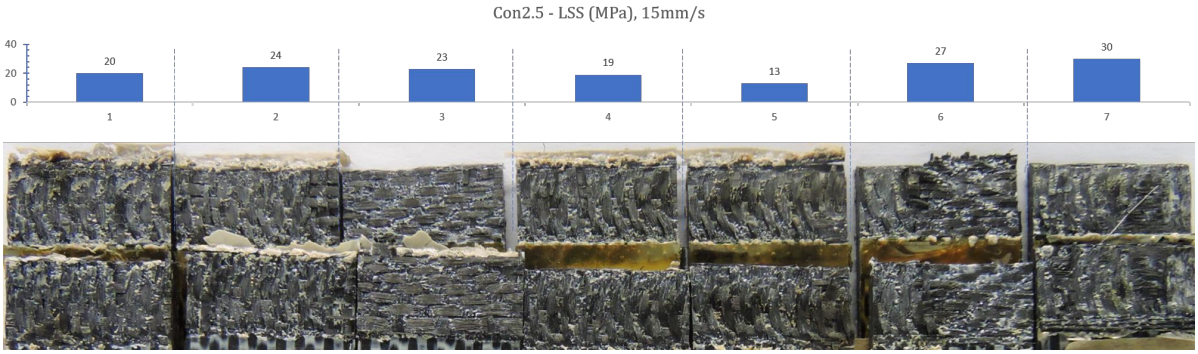

Figure 6.17: The fracture surfaces at a welding speed of 15mm/s

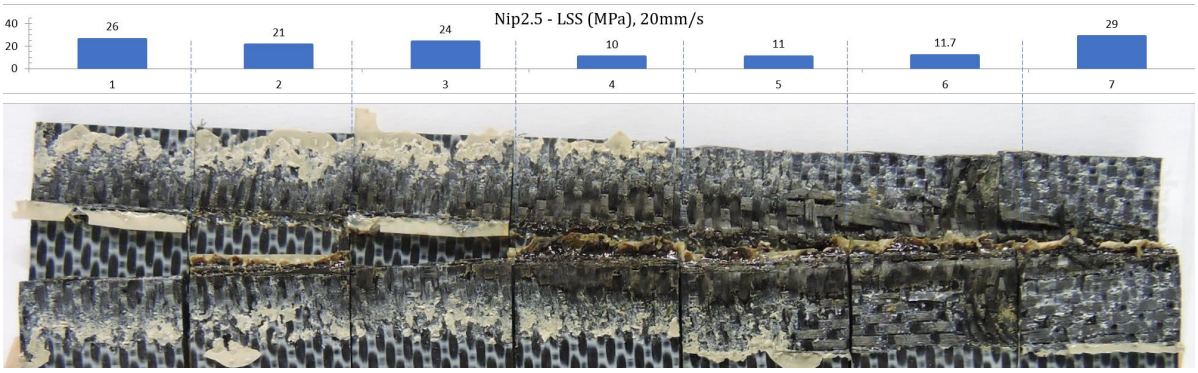

Figure 6.18: The fracture surfaces at a welding speed of 20mm/s

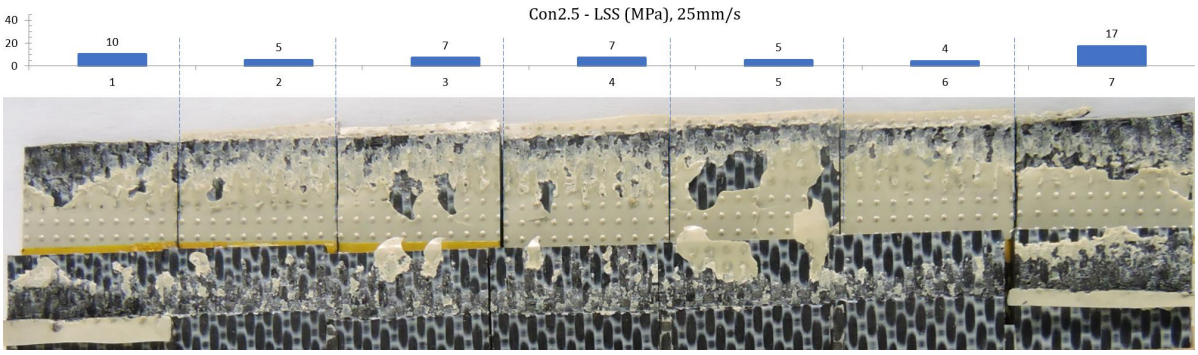

Figure 6.19: The fracture surfaces at a welding speed of 25mm/s

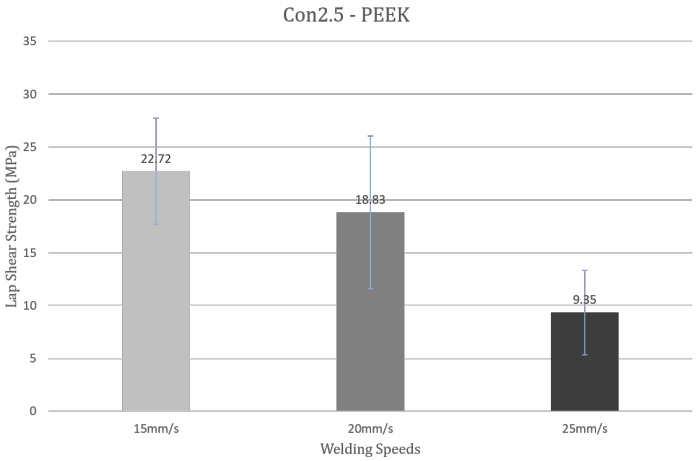

Figure 6.20: LSS of the Con2.5 PEEK ED

The single lap shear strengths of the Con2.5 ED after discarding the edge specimens (n=7) are shown in Fig.6.20 and Table6.4

Welding Speed	Lap Shear Strength
15 [mm/s]	22.72 ±5.01 [MPa]
20 [mm/s]	18.83 ±7.21 [MPa]
25 [mm/s]	8.15 ±4 [MPa]

Table 6.4: The lap shear strengths of the CUW specimens with a Con2.5 ED

Similar to the trend observed with the Con5 ED, the Con2.5 ED also showed an even heat generation at the interface, with no intact ED parts or burn marks. However, at a speed of 20mm/s there were portions of intact EDs at the start of the weld. And when the speed was increased to 25mm/s, this phenomenon was amplified, with majority of the ED remaining intact. There was melting only at one edge of the overlap, as shown in Fig.6.21

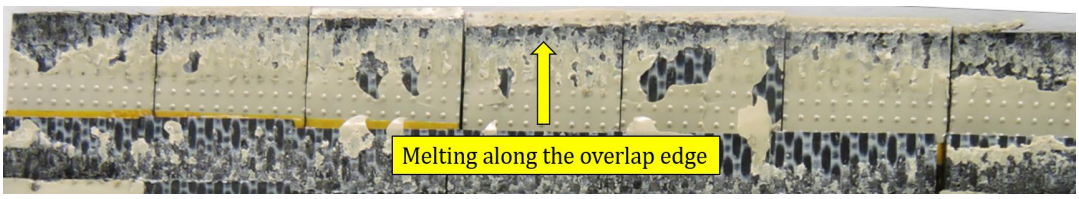

Figure 6.21: Fracture surface of the Con2.5 PEEK ED

As for the LSS values, a similar trend to Con5 ED was observed: highest strength at 15mm/s and the lowest at 25mm/s.

6.2. Data interpretation

From a general perspective, it was observed that different ED options showed a high LSS at different speeds. An overall comparison with the reference spot welds is shown in Fig.6.22

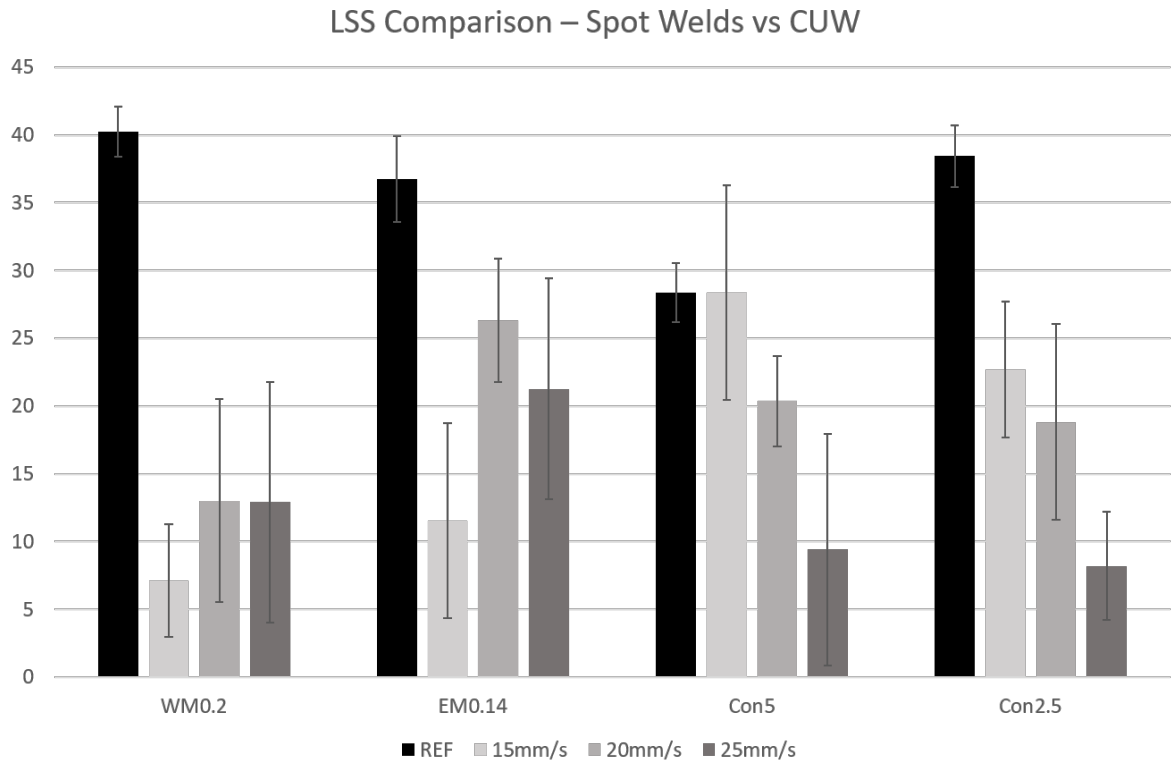

Figure 6.22: Comparison between the reference spot weld and CUW

As a primary observation, while the woven mesh seems to produce good results for a PPS to CF/PPS welding, for PEEK this does not seem to be the case. The resulting joints seemed to be at the extremes, with the speeds of 15mm/s causing overheating and the other speeds showing poor heat generation. The woven mesh also showed a lot of scatter across all the welding speeds, indicating that further research is needed to understand why the there is a mismatch when the material is changed from PPS to PEEK.

In order to find a trend between the obtained results and the properties of the EDs, the LSS was plotted against different features of the ED that were identified in the spot welds. It was assumed that during the CUW process, the conditions are similar to the spot welds.

6.2.1. Pre-forming vs LSS

To check if the pre-forming value during the spot welds had a direct effect on the LSS of the joint in CUW, the plot showed in Fig.6.23

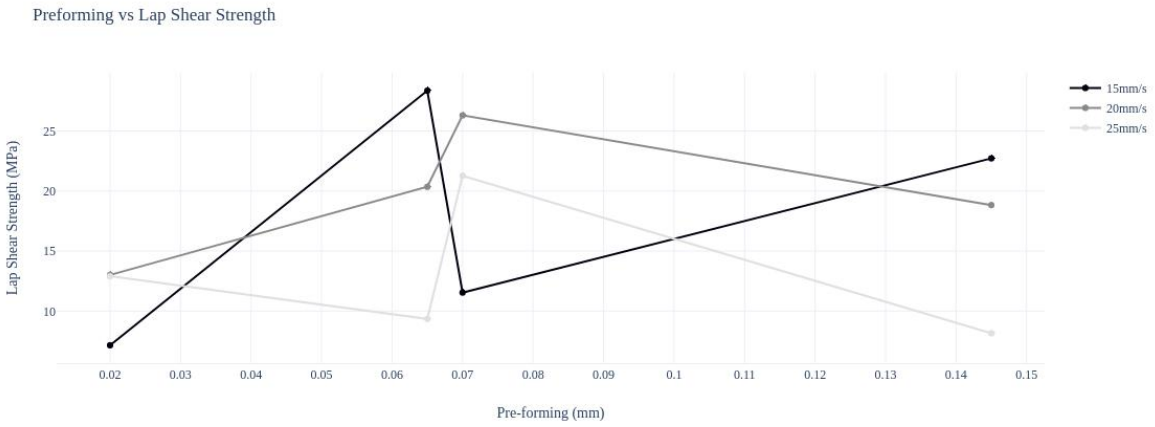

Figure 6.23: Pre-forming distance vs LSS

It can be seen in from the graph that the plots do not follow a particular trend over the different welding speeds. Two options that show a similar pre-forming value seem to show widely varying values of LSS at different welding speeds. Hence, the pre-forming from the spot welds does not seem to have a direct effect on the weld quality of at the interface, and there seems to be other factors at play.

6.2.2. Pre-forming time vs LSS

The next parameter that was checked was the pre-forming time observed in the spot welds, which is the time taken to reach the displacement plateau for the design. The plot is shown in Fig.6.24

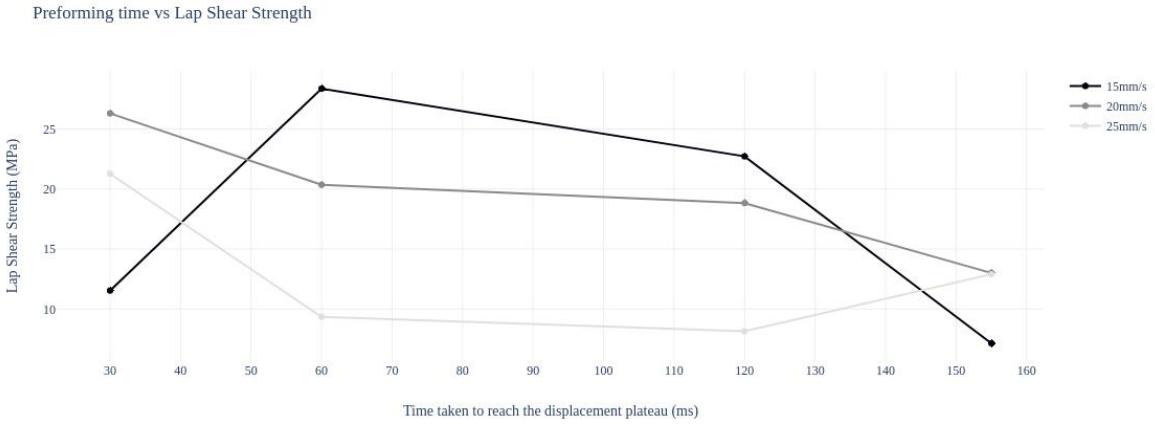

Figure 6.24: Pre-forming time vs LSS

At speeds of 20mm/s and 25mm/s, the LSS seems to slightly follow an inverse trend with the pre-forming time. This could possibly be an indication that if the ED is able to create an intimate contact faster, the weld quality is better as a result. However, this trend does not seem to apply in case of a welding speed of 15mm/s, with the expanded mesh showing a really low LSS while having the shortest preforming time. Hence, this is an indication of the fact that the pre-forming time alone does not have an effect on the weld quality.

6.2.3. Discussion

The pre-forming data from the spot welds does not seem to have a direct correlation to the observations made in the CUW process. This is probably due to the fact that when the sonotrode starts applying force at the start of the specimen, the entire top laminate pushes against the ED due to its stiffness. Hence, by the time the sonotrode reaches the unwelded area, the ED is already pre-formed.

Moreover, it is quite possible that as soon as the sonotrode starts welding at one end of the joint the vibrations also get transmitted throughout the weld line. This might increase the temperature throughout the weldline even before the sonotrode reaches the spot. This increase in temperature can possibly affect the stiffness of the ED, and in turn the preforming. Hence, in order to use the pre-forming data from the spot welds there has to be a better understanding of the actions taking place at the area around it.

6.2.4. Resin volume vs LSS

The volume of the resin in the ED could also probably contribute to the LSS. The plot in Fig.6.26 was generated to check this.

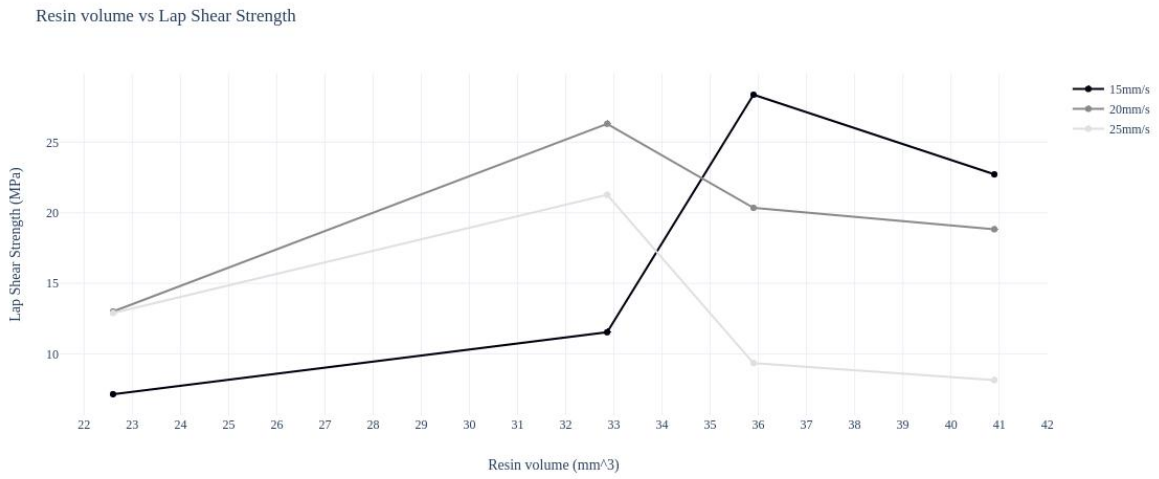

Figure 6.25: Resin volume vs LSS

The volume calculations are carried out for a 25.4mm x 12.7mm overlap, and are shown in the Appendix. It is observed that for all the welding speeds there seems to be a common trend where the curve reaches a peak and starts going low again. This trend could possibly imply that for every welding speed there exists a right volume of resin that gives the peak LSS. For welding speeds of 20mm/s and 25mm/s, the optimum resin volume seems to be around 33mm^3, while for a lower speed of 15mm/s it is around 35mm^3.

6.2.5. Expanded mesh vs Con5 ED

The 0.14mm thick expanded mesh and the Con5 ED offer a good comparison because of there almost similar volumes (32.86mm^3 & 35.9mm^3) and preforming values (0.07mm and 0.065mm).

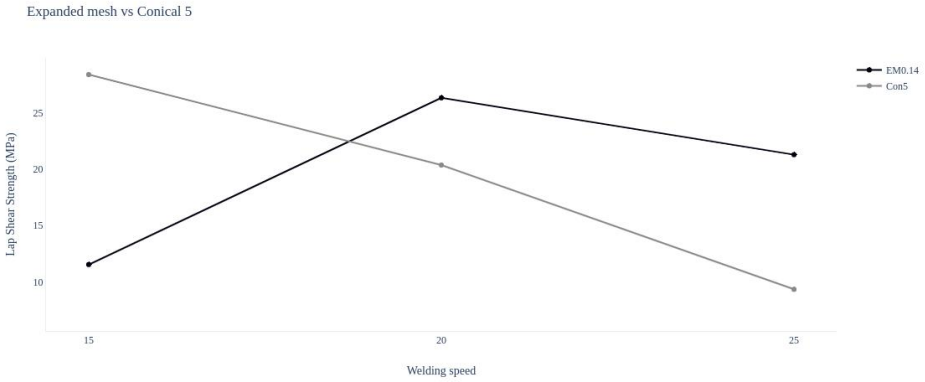

Figure 6.26: The variation in the LSS of the two EDs with respect to the welding speeds

The Con5 ED seems to have its peak LSS value at a welding speed of 15mm/s, while the expanded mesh peaks at a welding speed of 20mm/s. The structural aspect that differentiates the expanded mesh from the Con5 is the total surface area of the ED. This expanded mesh consists of a lot of thin strands connected to each other while the conical ED is a bit bulkier and solid with a lower total surface area. The thin strands in the expanded mesh probably create a higher welding pressure and are hence able to reach high temperatures faster compared to the Con5 ED. Hence, an expanded mesh works better at a higher speed than the Con5, which is capable of withstanding a higher amount of heat thanks to its bulkier structure.

6.2.6. Effect of number of contact points

Although the higher welding speed of 25mm/s resulted in poor strength joints for the Con5 and Con2.5 ED, the fracture surfaces give a good picture about the heat generation at the interface.

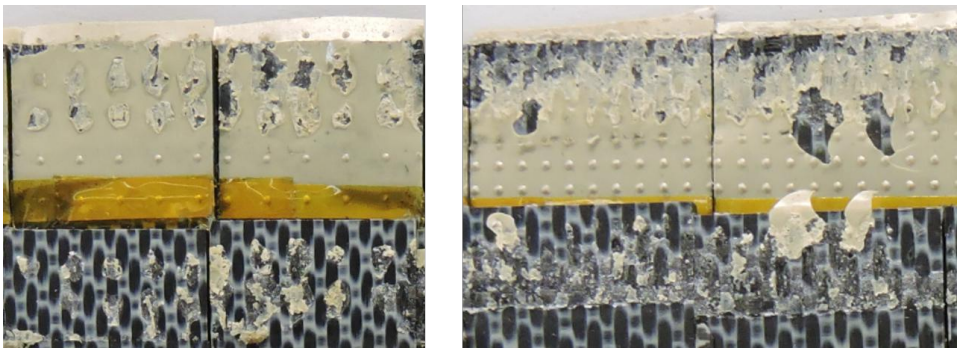

Figure 6.27: The fracture surfaces of Con5 (left) and Con2.5 (right) when welded at a speed of 25mm/s

Fig.6.27 shows that in case of Con5, only the cones of the ED start melting when the sonotrode passes by, but in case of Con2.5 the heat is effectively transferred to the base film due to which there is global melting. This is in accordance with the cross-sectional microscopic images seen in the previous chapter for this type of ED. This possibly implies that having more contact points in the ED will lead to a better heat generation at the interface.

6.3. Conclusions from the CUW

In this chapter, CUWs were carried out using the EDs evaluated in the previous chapter at three welding speeds: 15mm/s;20mm/s and 25mm/s. While the overall LSS of the specimens was low compared to the reference values, they did provide in understanding which features have an effect on the weld quality and which ones do not.

It was observed that the values of pre-forming distance and time in their own were not enough to affect the weld quality. It was then observed that the resin volume of the ED could be following a trend where for every welding speed, there is an optimum resin volume.

Next the expanded mesh and the Con5 ED were compared based on their welding speeds, and it was observed that although they have a similar volume and pre-forming, their LSS values peak at different welding speeds. It was implied that the total surface area of the ED could have a hand in this. Finally, it was shown that having more contact points leads to a more even and effective heat generation at the interface.

7

Conclusions

The aim of this research was to create an understanding of the energy directing surfaces at the interface and manufacture them for a continuous ultrasonic welding process.
Firstly the beneficial features for an energy directing surface for a CUW process were identified from the literature as:

- Small contact points
- Homogeneosly spread contact points
- Some deformation prior to welding

Then, different manufacturing options were explored to create new designs of energy directors that would likely exhibit these beneficial features. The FDM option, although partially successful in manufacturing EDs was later discarded owing to limited flexibility and build size. The moulding process was then tried and was successfully used to manufacture a conical ED. The conical ED seemed to incorporate the beneficial features discovered through the literature. After the proof of concept stage of the manufacturing process, a more precise version of the mould was made using CNC drill. In this new mould, two options could be manufactured: one with the cones 5mm apart and cones 2.5mm apart.
The next step was to evaluate and characterize these EDs by using them for spot welds. The power-displacement data from these tests gives information about the pre-forming and the time taken to reach the pre-forming plateau. The power-displacement curves are also used to identify the weld time for optimum LSS for each ED. The weld time for the conical EDs was also identified using the same technique for meshes, and was found to be sub-optimal as the fracture surface had intact ED, resulting in a lower than average LSS value for Con5.
For the continuous ultrasonic welding, the four EDs used were:

- Woven mesh
- Expanded mesh
- Con5
- Con2.5

For the sake of comparison, the material used in all the EDs was limited to PEEK. The welds were performed at three different speeds: 15mm/s; 20mmm/s and 25mm/s over 220mm long specimens. were evaluated at three different speeds. It was observed that different energy directors produce desirable results at different welding speeds depending on their physical features. Although a main criteria that decides the quality of a CUW could not be established, some features like the resin volume and preforming time seemed to have a effect that can be quantified with further research. Then, it was hypothesized that the surface area of an ED has a positive effect in the melting time of the EDs.

It was observed that two EDs (Expanded mesh and Con5), with similar volume and preforming reached their best at different welding speeds. Finally, the positive effect of having higher contact points on the heat generation was shown.
As a whole, this thesis creates an understanding of which features of an ED affect a CUW process, and how the information from spot welds could be used to characterize an ED for the process. It shows that with proper research, the process can be well controlled to create high quality welds in the future.

7.1. Revisiting the research questions

It is perhaps a good idea to know how the research work fared in terms of the research objectives that were set in the beginning.

- What are the desirable features in an ED for a CUW process?
  It was identified from the literature that having small, homogeneously spread contact areas are beneficial for a good weld uniformity. It was observed with the PEEK woven mesh that the results seen for woven PPS EDs, do not translate exactly to a PEEK ED.
- How can these features be incorporated into a new design?
  The beneficial features identified through literature were successfully applied into a new design and manufactured at the laboratory. One of the resulting EDs(Con5) showed an acceptable uniformity at a speed of 20mm/s.
- What are the relations between the physical features of an ED and the weld uniformity?
  First, it was seen preforming, which is a result of the physical features of the ED, could not be directly related to the weld quality as a numeric property. It was later observed that for the same resin volume, the LSS can be different depending on the structural properties of the ED. A higher total surface area showed a higher LSS at a faster speed, where as a conical structure showed a higher LSS at a slower speed for a similar resin volume

7.2. Recommendations for future research

During the course of this research, several areas that could be researched upon popped up:

- Although FDM process for manufacturing loose EDs sounds time consuming for the manufacturers, this technique is quite handy for researchers who need to make a one-off design for research. It could be interesting to see if this process could be optimized further to improve the quality of the end product.
- In this research, an attempt was made to estimate the preforming of the conical ED through an analytical approach. If this kind of EDs ever start being used widely, it would be good to have an approach that estimates the preforming
- During the CUW process, a lot of damage to the topmost layer was noticed because of the moving sonotrode. This probably calls for a consolidation device that follows the sonotrode and repairs the trail behind it.
- As of now, the power-displacement data from the CUW machine is not being evaluated due to insufficient understanding of the process. If they can be decoded, this data could add a lot of value to the knowledge in this field.

A

Appendix

A.1. ED volume calculations

A.1.1. Woven mesh

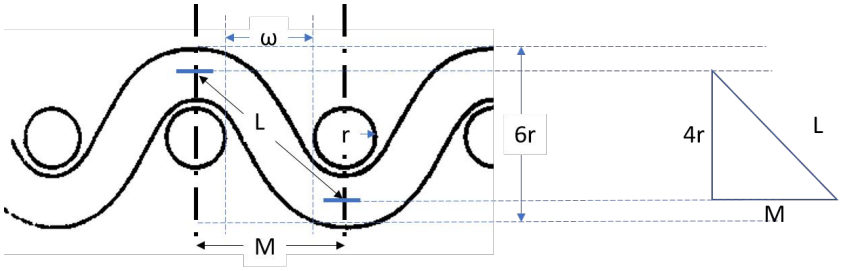

Figure A.1: A cross-section of the woven mesh with all the dimensions shown

Fig.A.1 shows the dimensions used in the calculation of the volume of the woven mesh ED. The mesh parameters are shown below:

$$\omega = \text{Mesh opening} = 154\mu m$$
$$r = \text{Filament radius} = 50\mu m$$
$$\text{Mesh count} = \text{Warp/Weft} = 39/39$$

The mesh section shown in Fig.A.1 is simplified into a right angled triangle with sides 4r, L and M. The dimensions L and M are calculated as:

$$M = \omega + 2r = 154 + 2 * 50 = 254\mu m$$
$$L = \sqrt{M^2 + (4r)^2} = \sqrt{254^2 + (4 * 50)^2} = 323.3\mu m$$

This basically means that between two adjacent threads, the filament length L is roughly 323.3µm. As per the mesh count, there are 39 threads per 1cm. This means that there are 38 Ls between the 39 threads along 1cm of the mesh. Hence, along 1cm of the mesh the length of the filament is given by

$$L_{1cm} = 323.3 * 38 = 12285.4\mu m$$

The volume of the filament over 1cm of length is then given by

$$V_{1cm} = \pi * r^2 * L_{1cm} = \pi * 50^2 * 12285.4 = 96489305.97\mu m^3$$

The volume of 1 filament over a length of 2.54 cm and 1.27cm respectively, is then calculated as:

$$V_{2.54cm} = 96489305.97 * 2.54 = 245082837.15\mu m^3 = 0.245mm^3$$

$$V_{1.27cm} = V_{2.54cm}/2 = 0.122mm^3$$

The number of filaments along the overlap can then be calculated for each side of the mesh. Along the 2.54cm side of the overlap, there will be 39*2.54(=approx. 100) filaments of volume $V_{1.27}$ and similarly along the 1.27cm side of the overlap, there will be 39*1.27(=approx. 50) filaments of volume $V_{2.54}$. The total volume is therefore given by

$$V_{overlap} = 100 * 0.122 + 50 * 0.245 = 24.5mm^3$$

A.1.2. Expanded mesh

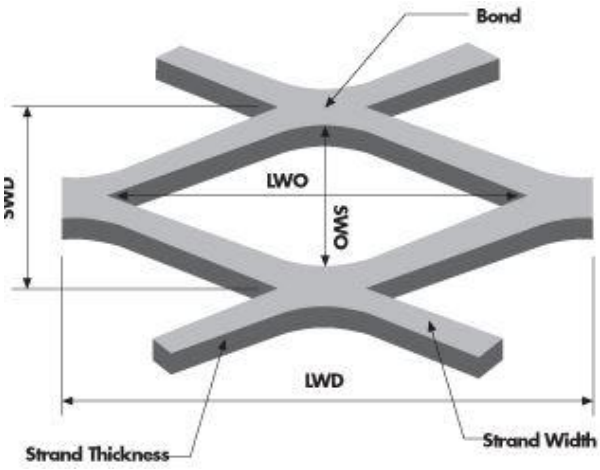

Figure A.2: The dimensions of an expanded mesh[8]

The different dimensions of an expanded mesh are shown in Fig.A.2. From the supplier data sheet, the following data is obtained:

$$\begin{aligned} SWO &= 0.008" = 0.20mm \\ LWO &= 0.0185" = 0.47mm \\ SWD &= 0.0185" = 0.47mm \\ LWD &= 0.031" = 0.79mm \\ Mesh\ thickness &= 0.0055" = 0.1397mm \end{aligned}$$

The area of the resin's surface area is calculated by dividing every diamond into a separate section and then calculating the amount of resin cover in every section. Every section is a rectangle of dimensions LWD x SWD. The open area in every section is a rhombus of diagonals SWO and LWO added with another rhombus of the same dimensions that has been split into four equal parts. Hence, the total resin area is then calculated by subtracting the area of the two rhombuses from the area of the main section.

$$A_{resin} = SWD * LWD - (\frac{1}{2} * SWO * LWO) * 2 = (0.47 * 0.787) - (0.20 * 0.47) = 0.274mm^2$$

Along a length of 25.4mm, there are 25.4/LWD number of sections and along the length of 12.7, there are 12.7/SWD number of sections. (Assuming that the LWDs were placed parallel to the 25.4mm side). This means there are total number of sections are:

$$Number\ of\ sections\ along\ the\ length\ = 25.4/0.787 = 32.25\ sections$$

$$Number\ of\ sections\ along\ the\ width\ = 12.7/0.47 = 27.02\ sections$$

$$Total\ number\ of\ sections\ in\ the\ overlap\ = 32.25 * 27.02 = 871.4\ sections$$

Hence, the total resin area is then given by

$$Total\ resin\ area\ = A_resin * 871.4 = 235.28mm^2$$

The total resin volume is then given by multiplying it with the mesh thickness:

$$Total\ Volume = 235.28 * 0.1397 = 32.86mm^3$$

A.1.3. Conical ED

The volume calculation for the conical ED is carried out by adding the volume of the base film and the volume of the cones.

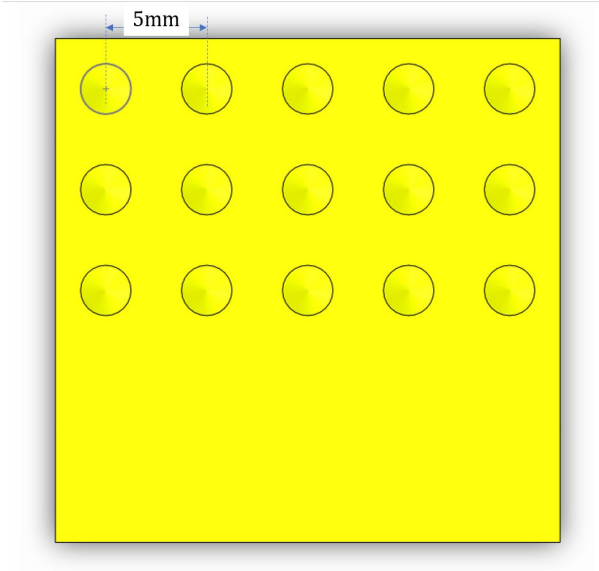

Figure A.3: Con 5 ED for reference

The thickness of the base sheet is measured along 4 different points in the edges using a screw gauge, and is found to be approximately 0.11mm. Similarly, the cone heights are measured and the base sheet thickness is then subtracted to attain the value of the height of the cone(=0.21mm). The cone radius is then calculated using trigonometric ratios, since the cone angle is known(r=0.5067). The volume of the base film is calculated as:

$$V_{base} = Area_{overlap} * thickness = 25.4 * 12.7 * 0.11 = 35.48mm^3$$

The heights of one cone is given by

$$V_{cone} = \frac{\pi}{3} * r^2 * h = \frac{\pi}{3} * (0.5067)^2 * 0.21 = 0.0565mm^3$$

In case of the Con5, there are 10 such cones in the overlap, and in case of the Con2.5, there are 20.

Volume of the Con5 ED

$$V_{con5} = V_{base} + 10 * V_{cone} = 35.48 + 10 * 0.0565 = 35.9mm^3$$

Volume of the Con2.5 ED

$$V_{con2.5} = V_{base} + 20 * V_{cone} = 35.48 + 20 * 0.0565 = 36.9mm^3$$

A.2. Derivation for the analytical relation between the cone height and preforming

Assuming that the resin flow fronts from the molten cones meet each other to form a new layer while the base film layer stays intact as shown in Fig.A.4, an attempt was made to find a relation between the pre-forming and the cone height.

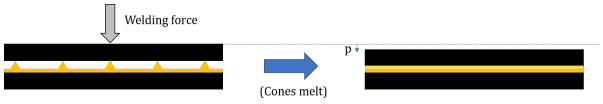

Figure A.4: The cones melting to form a new layer at the interface

The total resin volume before and after the melting process remains the same. The following parameters are introduced:

$$h_c = height\ of\ the\ cone$$
$$r_c = radius\ of\ the\ cone = h_c/tan(23.5) = h_c/0.435$$
$$p = preforming$$
$$h_m = height\ of\ the\ molten\ resin\ layer$$
$$n = number\ of\ cones$$
$$V_c = Volume\ of\ a\ cone$$
$$V_m = Volume\ of\ the\ molten\ resin\ layer$$

After the melting process, the following relation can be established:

$$h_c = p + h_c$$

Since it is assumed that only the cones melt and the base layer stays intact, the volume of the cones gets converted into the new molten resin layer:

$$n * V_c = V_m$$
$$n * \frac{\pi}{3} * r_c^2 * h_c = 25.4 * 12.7 * h_m$$
$$n * \frac{\pi}{3}(h_c/0.435)^2 * h_c = (322.6) * (h_c - p)$$
$$n * 5.534 * h_c^3 = 322.6(h_c - p)$$
$$n(0.017)h_c^3 = h_c - p$$

Thus, we arrive at the equation

$$p = h_c = 0.017 * n * h_c^3$$

A.2.1. Estimation of the welding speed

The fracture surfaces from two tests using a 0.14mm thick expanded mesh are shown in Fig.A.5

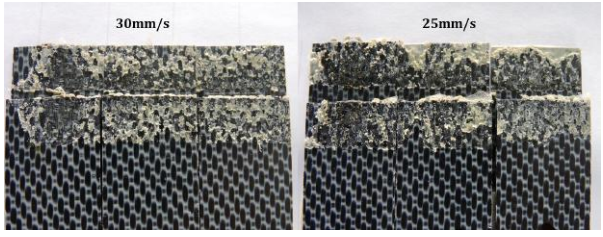

Figure A.5: The fracture surface at a speed of 30mm/s(left) and the fracture speed of 25mm/s(right)

In both the cases, there was a lot of intact resin visible, which was an indication that the heat generation at the interface was not sufficient. To tackle this, 3 lower welding speeds were tested for the main comparison: 15mm/s, 20mm/s and 25mm/s.

Bibliography

[1] Security of Supply. Technical report. URL https://www.victrex.com/~/media/literature/en/victrex_pps_fp_replacement-flyer_final.pdf.

[2] A. Benatar. Ultrasonic welding of plastics and polymeric composites. *Power Ultrasonics*, pages 295–312, 1 2015. doi: 10.1016/B978-1-78242-028-6.00012-0. URL https://www.sciencedirect.com/science/article/pii/B9781782420286000120.

[3] Avraham Benatar and Timothy G. Gutowski. Ultrasonic welding of PEEK graphite APC-2 composites. *Polymer Engineering and Science*, 29(23):1705–1721, 12 1989. ISSN 0032-3888. doi: 10.1002/pen.760292313. URL http://doi.wiley.com/10.1002/pen.760292313.

[4] Yew Khoy Chuah, Liang-Han Chien, B. C. Chang, and Shih-Jung Liu. Effects of the shape of the energy director on far-field ultrasonic welding of thermoplastics. *Polymer Engineering & Science*, 40(1):157–167, 1 2000. ISSN 0032-3888. doi: 10.1002/pen.11149. URL http://doi.wiley.com/10.1002/pen.11149.

[5] Dexmet Corporation. Expanded material terminology, 2019.

[6] Dukane Corporation. What Happened to Your Ultrasonic Weld Quality? | Dukane. URL https://www.dukane.com/what-happened-to-your-ultrasonic-weld-quality/.

[7] Engineering Toolbox. Coefficients of Linear Thermal Expansion. URL https://www.engineeringtoolbox.com/linear-expansion-coefficients-d_95.html.

[8] Grating Pacific. Expanded Metal - Nomenclature. URL http://www.gratingpacific.com/expanded_metals/expanded_metals_specifications.html.

[9] D Grewell and A Benatar. Welding of Plastics: Fundamentals and New Developments. Technical report. URL https://pdfs.semanticscholar.org/df1f/a82c86009da287842716da8655f31a1c5721.pdf.

[10] B.C.P. Jongbloed, J.J.E. Teuwen, Genevieve Palardy, and Irene Fernandez Villegas. Improving weld uniformity in continuous ultrasonic welding of thermoplastic composites. *ECCM18: 18th European Conference on Composite Materials*, 2018. URL https://repository.tudelft.nl/islandora/object/uuid%3A22b7283a-71c1-4fdf-80db-1008ac98c076.

[11] K. Jud, H. H. Kausch, and J. G. Williams. Fracture mechanics studies of crack healing and welding of polymers. *Journal of Materials Science*, 16(1):204–210, 1 1981. ISSN 0022-2461. doi: 10.1007/BF00552073. URL http://link.springer.com/10.1007/BF00552073.

[12] Ties Kerssemakers. Investigating the use of Fused Deposition Modeling as Energy Director application method for Ultrasonic Welding of Thermoplastic Composites, 2018. URL https://repository.tudelft.nl/islandora/object/uuid%3Ac4832568-700d-4db2-a680-ebf67f170903.

[13] Omar A. Mohamed, Syed H. Masood, and Jahar L. Bhowmik. Optimization of fused deposition modeling process parameters: a review of current research and future prospects. *Advances in Manufacturing*, 3(1):42–53, 3 2015. ISSN 2095-3127. doi: 10.1007/s40436-014-0097-7. URL http://link.springer.com/10.1007/s40436-014-0097-7.

[14] G. Palardy and Irene Fernandez Villegas. Ultrasonic welding of thermoplastic composites with flat energy directors: Influence of the thickness of the energy director on the welding process. *ICCM 20: 20th International Conference on Composite Materials, Copenhagen, Denmark, 19-24 July 2015*, 2015. URL https://repository.tudelft.nl/islandora/object/uuid%3A20fef8a5-a64b-4eff-9b92-730ccdf6a634.

[15] H. Potente. Ultrasonic welding — Principles & theory. *Materials & Design*, 5(5):228–234, 10 1984. ISSN 0261-3069. doi: 10.1016/0261-3069(84)90032-3. URL https://www.sciencedirect.com/science/article/pii/0261306984900323.

[16] SOLOFF ETAL R, S. METHOD OF BONDING NON-THERMOPLASTIC PARTS BY SONIC ENERGY, 1966. URL https://patentimages.storage.googleapis.com/22/73/2a/37e1242428ab84/US3284257.pdf.

[17] Ryonet Corporation. How to Choose the Right Screen Mesh Size | Screen-Printing.com by Ryonet. URL https://www.screenprinting.com/pages/screen-printing-mesh-size-information.

[18] Alex Savitski, Hardik Pathak, Leo Klinstein, Mike Luehr, Paul Golko, and Kenneth Holt. A Case for Round Energy Director * : Utilizing Advanced Control Capabilities of Servo-Driven Ultrasonic Welders in Evaluating Round Energy Director Performance .

[19] F.J.M. Senders. Continuous Ultrasonic Welding of Thermoplastic Composites, 2016. URL https://repository.tudelft.nl/islandora/object/uuid%3A26e5fa99-6fd2-425b-937e-c596ba79cc6a.

[20] Frank Senders, Martijn van Beurden, Genevieve Palardy, and Irene Fernandez Villegas. Zero-flow: a novel approach to continuous ultrasonic welding of CF/PPS thermoplastic composite plates. *Advanced Manufacturing: Polymer & Composites Science*, 2(3-4):83–92, 10 2016. ISSN 2055-0340. doi: 10.1080/20550340.2016.1253968. URL https://www.tandfonline.com/doi/full/10.1080/20550340.2016.1253968.

[21] A. Shoh. Welding of thermoplastics by ultrasound. *Ultrasonics*, 14(5):209–217, 9 1976. ISSN 0041-624X. doi: 10.1016/0041-624X(76)90020-2. URL https://www.sciencedirect.com/science/article/pii/0041624X76900202.

[22] The Welding Institute. Ultrasonic welding of injection moulded components - Part 1 - Process and equipment - Job Knowledge 61 - TWI. URL https://www.twi-global.com/technical-knowledge/job-knowledge/ultrasonic-welding-of-injection-moulded-components-part-1-process-and-equipment-

[23] M.Q.C. Van Beurden. Development & assessment of equipment and procedure for continuous ultrasonic welding of thermoplastic composites, 2015. URL https://repository.tudelft.nl/islandora/object/uuid%3Af2dd2a05-f7d7-4b22-92c6-cc04e2499780.

[24] Irene Fernandez Villegas. Optimum Processing Conditions For Ultrasonic Welding Of Thermoplastic Composites. *The 19th International Conference on Composite Materials*, pages 1–8, 2013. URL http://confsys.encs.concordia.ca/ICCM19/AllPapers/FinalVersion/FER80442.pdf.

[25] Irene Fernandez Villegas. In situ monitoring of ultrasonic welding of thermoplastic composites through power and displacement data. *Journal of Thermoplastic Composite Materials*, 28(1):66–85, 1 2015. ISSN 0892-7057. doi: 10.1177/0892705712475015. URL http://journals.sagepub.com/doi/10.1177/0892705712475015.

[26] Irene Fernandez Villegas and Harald E. N. Bersee. Ultrasonic welding of advanced thermoplastic composites: An investigation on energy-directing surfaces. *Advances in Polymer Technology*, 29(2):112–121, 7 2010. ISSN 07306679. doi: 10.1002/adv.20178. URL http://doi.wiley.com/10.1002/adv.20178.

[27] Irene Fernandez Villegas and Genevieve Palardy. Ultrasonic welding of CF/PPS composites with integrated triangular energy directors: melting, flow and weld strength development. *Composite Interfaces*, 24(5):515–528, 6 2017. ISSN 0927-6440. doi: 10.1080/09276440.2017.1236626. URL https://www.tandfonline.com/doi/full/10.1080/09276440.2017.1236626.

[28] Xiaolin Wang, Jiuchun Yan, Ruiqi Li, and Shiqin Yang. FEM Investigation of the Temperature Field of Energy Director During Ultrasonic Welding of PEEK Composites. *Journal of Thermoplastic Composite Materials*, 19(5):593–607, 9 2006. ISSN 0892-7057. doi: 10.1177/0892705706067479. URL http://journals.sagepub.com/doi/10.1177/0892705706067479.

[29] Ali Yousefpour, Mehdi Hojjati, and Jean-Pierre Immarigeon. Fusion Bonding/Welding of Thermoplastic Composites. *Journal of Thermoplastic Composite Materials*, 17(4): 303–341, 7 2004. ISSN 0892-7057. doi: 10.1177/0892705704045187. URL http://journals.sagepub.com/doi/10.1177/0892705704045187.

[30] Tian Zhao, Genevieve Palardy, Irene Fernandez Villegas, Calvin Rans, Marcias Martinez, and Rinze Benedictus. Mechanical behaviour of thermoplastic composites spot-welded and mechanically fastened joints: A preliminary comparison. *Composites Part B: Engineering*, 112:224–234, 3 2017. ISSN 1359-8368. doi: 10.1016/J.COMPOSITESB.2016.12.028. URL https://www.sciencedirect.com/science/article/pii/S1359836816321126.